Electroweak radiative corrections to W boson production in hadronic collisions

U. Baur
Department of Physics, State University of New York, Buffalo, New York 14260

S. Keller
Theory Group, Fermi National Accelerator Laboratory, Batavia, Illinois 60510

D. Wackeroth
F1 Theory Group, Paul Scherrer Institute, CH-5232 Villigen PSI, Switzerland
(Received 20 July 1998; published 19 November 1998)

The $\mathcal{O}(\alpha)$ electroweak radiative corrections to the process $p\overset{(-)}{p}\to W^{\pm}\to \ell^{\pm}\nu$ ($\ell=e,\mu$) are calculated. The $\mathcal{O}(\alpha)$ corrections can be decomposed into separate gauge invariant contributions to the W boson production and decay processes. Factorizing the collinear singularity associated with initial state photon radiation into the parton distribution functions, we find that initial state corrections have a significantly smaller effect than final state radiative corrections. We study in detail the effect of electroweak radiative corrections on a number of interesting observables: the W transverse mass distribution, the W to Z transverse mass ratio, the charge asymmetry of leptons in $W\to\ell\nu$ decays, as well as the W production cross section and the W to Z cross section ratio. We also investigate how experimental lepton identification requirements change the effect of the electroweak corrections. [S0556-2821(98)03823-5]

PACS number(s): 12.15.Lk, 13.38.Be, 13.85.Qk, 14.70.Fm

I. INTRODUCTION

The standard model (SM) of electroweak interactions so far has met all experimental challenges and is now tested at the 0.1% level [1]. However, there is little direct experimental information on the mechanism which generates the masses of the weak gauge bosons. In the SM, spontaneous symmetry breaking is responsible for mass generation. The existence of a Higgs boson is a direct consequence of this mechanism. At present the negative result of direct searches performed at the CERN e^+e^- collider LEP2 imposes a lower bound of $M_H>87.6$ GeV [2] on the Higgs boson mass. Indirect information on the mass of the Higgs boson can be extracted from the M_H dependence of radiative corrections to the W boson mass, M_W, and the effective weak mixing angle, $\sin^2\theta_{\rm eff}^{\rm lept}$. Assuming the SM to be valid, a global χ^2 fit to all available electroweak precision data yields a (one-sided) 95% confidence level (C.L.) upper limit on M_H of 408 GeV [3].

Future more precise measurements of M_W and the top quark mass, $m_{\rm top}$, will lead to more accurate information on the Higgs boson mass [4–6]. Currently, the W boson mass is known to ± 65 MeV [7] from direct measurements, whereas the uncertainty of the top quark mass is ± 5.2 GeV [8]. With a precision of 30 MeV (10 MeV) for the W mass, and 2 GeV for the top quark mass, M_H can be predicted from a global analysis with an uncertainty of about 30% (15%) [5,6]. Comparison of these indirect constraints on M_H with the results from direct Higgs boson searches at LEP2, the Fermilab Tevatron collider, and the CERN Large Hadron Collider (LHC) will be an important test of the SM. They will also provide restrictions on the parameters of the minimal supersymmetric extension of the standard model (MSSM) [9].

A significant improvement in the W mass uncertainty is expected in the near future from measurements at LEP2 [10] and the Fermilab Tevatron $p\overline{p}$ collider [5]. The ultimate precision expected for M_W from the combined LEP2 experiments is approximately 40 MeV [10]. At the Tevatron, integrated luminosities of the order 1 fb^{-1} are envisioned in the Main Injector Era (run II), and one expects to measure the W mass with a precision of approximately 50 MeV [5] per experiment. The prospects for a precise measurement of M_W would further improve if a significant upgrade in luminosity beyond the goal of the Main Injector could be realized. With recent advances in accelerator technology [11], Tevatron collider luminosities of the order 10^{33} cm^{-2} s^{-1} may become a reality, resulting in integrated luminosities of up to 10 fb^{-1} per year. With a total integrated luminosity of 30 fb^{-1}, one can target a precision of the W mass of 15–20 MeV [5]. A similar or better accuracy may also be reached at the LHC [12].

In order to measure the W boson mass with high precision in a hadron collider environment, it is necessary to fully understand and control higher order QCD and electroweak (EW) corrections. A complete calculation of the full $\mathcal{O}(\alpha)$ electroweak radiative corrections to $p\overset{(-)}{p}\to W^{\pm}\to\ell^{\pm}\nu$ ($\ell=e,\mu$) has not been carried out yet. In a previous calculation, only the final state photonic corrections were included [13,14], using an approximation in which the sum of the soft and virtual parts is indirectly estimated from the inclusive $\mathcal{O}(\alpha^2)$ $W\to\ell\nu(\gamma)$ width and the hard photon bremsstrahlung contribution. The unknown part of the $\mathcal{O}(\alpha)$ electroweak radiative corrections, combined with effects of multiple photon emission (higher-order corrections), have been estimated to contribute a systematic uncertainty of $\delta M_W=15-20$ MeV to the measurement of the W mass [15,16].

In this paper we present a new and more accurate calculation of the $\mathcal{O}(\alpha)$ EW corrections to resonant W boson production in hadronic collisions. Our calculation is based on the full set of $\mathcal{O}(\alpha^3)$ Feynman diagrams, and includes both initial and final state radiative corrections, as well as the contributions from their interference. Final state charged lep-

ton mass effects are included in the following approximation. The lepton mass regularizes the collinear singularity associated with final state photon radiation. The associated mass singular logarithms of the form $\ln(\hat{s}/m_{\ell}^2)$, where $\hat{s}$ is the squared parton center of mass energy and m_{ℓ} is the charged lepton mass, are included in our calculation, but the very small terms of $\mathcal{O}(m_{\ell}^2/\hat{s})$ are neglected.

To perform our calculation, we use a Monte Carlo method for next-to-leading-order (NLO) calculations similar to that described in Ref. [17]. With the Monte Carlo method, it is easy to calculate a variety of observables simultaneously and to simulate detector response. Calculating the EW radiative corrections to resonant W boson production, the problem arises how an unstable charged gauge boson can be treated consistently in the framework of perturbation theory. This problem has been studied in Ref. [18] with particular emphasis on finding a gauge invariant decomposition of the EW $\mathcal{O}(\alpha)$ corrections into a QED-like and a modified weak part. Unlike the Z boson case, the Feynman diagrams which involve a virtual photon do not represent a gauge invariant subset. In Ref. [18], it was demonstrated how gauge invariant contributions that contain the infrared (IR) singular terms can be extracted from the virtual photonic corrections. These contributions can be combined also with the IR-singular real photon corrections in the soft photon region to form IR-finite gauge invariant QED-like contributions corresponding to initial state, final state and interference corrections. The collinear singularities associated with initial state photon radiation can be removed by universal collinear counter terms generated by ''renormalizing'' the parton distribution functions [19,20], in complete analogy to gluon emission in QCD. A similar strategy has been employed in a recent calculation of the $\mathcal{O}(\alpha)$ QED corrections to Z boson production in hadronic collisions [21].

The technical details of our calculation are described in Sec. II. We first extract the collinear behavior of the partonic cross section for both the initial and the final state corrections. Then, we define the quark distribution functions in next-to-leading order QED within the QED deep inelastic scattering (DIS) and the QED modified minimal subtraction ($\overline{\text{MS}}$) factorization scheme when a finite quark mass is used to regulate the collinear singularities. Finally, we provide explicit formulas for the $\mathcal{O}(\alpha^3)$ differential cross section and perform various consistency checks.

Numerical results for $p\overline{p}$ collisions at $\sqrt{s}=1.8$ TeV are presented in Sec. III. In hadron collider experiments, W bosons are identified by their leptonic decays, $W\to\ell\nu$. Since the neutrino escapes undetected, the $\ell\nu$ invariant mass cannot be reconstructed, and one must resort to other kinematic variables for the measurement of M_W. The observable which currently provides the best measurement of M_W is the distribution of the transverse mass, M_T. The M_T distribution sharply peaks at M_W, and is rather insensitive to QCD corrections [22]. Alternative measurements of the W mass are provided [16] by the lepton p_T distribution which peaks at $M_W/2$, and the W/Z transverse mass ratio [23,24]. Because of the mass singular logarithms associated with final state photon bremsstrahlung in the limit where the photon is emitted collinear with the charged lepton, the distributions which are sensitive to M_W, the W production cross section and the W to Z cross section ratio in presence of cuts, and the charge asymmetry of leptons in W decays are significantly affected by the $\mathcal{O}(\alpha)$ electroweak radiative corrections.

The size of the radiative corrections strongly depends on the detector resolution. In Sec. III, using a simplified model of the DØ detector as an example, we also investigate how the finite resolution of realistic detectors affects the electroweak radiative corrections. Electrons and photons which are almost collinear are difficult to discriminate, and the momenta of the two particles are thus recombined into an effective electron momentum [15,16] if their separation in the pseudorapidity—azimuthal angle plane is below a critical value. This procedure completely eliminates the mass singular logarithms and, therefore, strongly reduces the size of the $\mathcal{O}(\alpha)$ corrections. In contrast, photons which are almost collinear with muons are rejected if they are too energetic [15,25] which results in residual mass singular logarithmic corrections to observable quantities in W production. Finally, our conclusions are presented in Sec. IV.

II. $\mathcal{O}(\alpha)$ ELECTROWEAK CORRECTIONS TO W PRODUCTION IN HADRONIC COLLISIONS

The calculation presented here employs a combination of analytic and Monte Carlo integration techniques.[1] Details of the method can be found in Ref. [17]. The Feynman diagrams contributing to W boson production in hadronic collisions to $\mathcal{O}(\alpha^3)$,

$$q_i(p_i)\overline{q}_{i'}(p_{i'})\to W^+(q)(\gamma)\to \nu_{\ell}(p_f)\ell^+(p_{f'})(\gamma(k))$$

are shown in Fig. 1. Since we are interested in the cross sections in the vicinity of the W resonance, the W,Z box diagrams can be neglected as nonresonant contributions of higher order in perturbation theory, and thus are not depicted in Fig. 1. The calculation of $\ell\nu$ production in hadronic collisions at $\mathcal{O}(\alpha^3)$ includes contributions from the square of the Born graphs, the interference between the Born diagrams and the virtual one-loop graphs, and the square of the real emission diagrams.

Our treatment of the $\mathcal{O}(\alpha)$ corrections to W boson production in the resonance region is based on the calculation presented in Ref. [18], which we outline here. Unlike the Z boson case, the Feynman diagrams of Fig. 1 which involve a virtual photon do not represent a gauge invariant subset. In Ref. [18], it was demonstrated how gauge invariant contributions that contain the infrared singular terms can be extracted from the virtual photonic corrections. These contributions can be combined with the also IR-singular real photon corrections in the soft photon region to form IR-finite gauge invariant QED-like contributions corresponding to initial

[1] A parton level Monte Carlo program (in FORTRAN) for $p\overset{(-)}{p}\to W^{\pm}\to\ell^{\pm}\nu$ including $\mathcal{O}(\alpha)$ EW corrections is available from http://ubhex.physics.buffalo.edu/~baur/wgrad/wgrad.tar.gz, or by contacting baur@ubhex.physics.buffalo.edu.

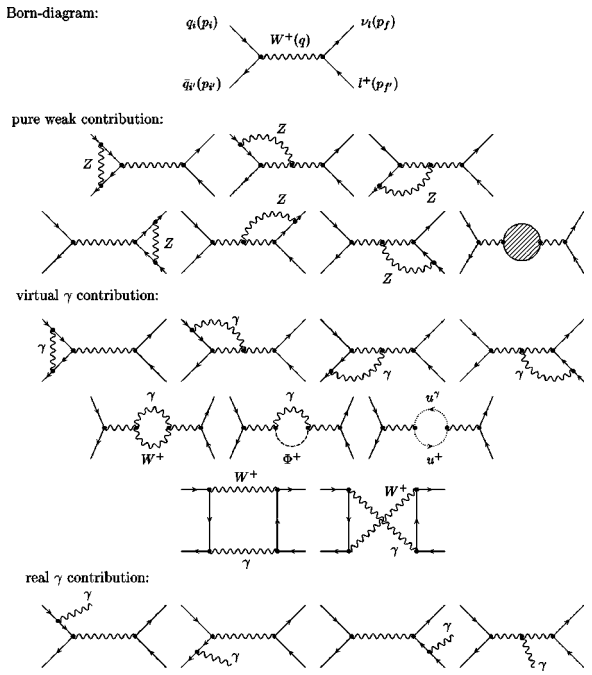

FIG. 1. The Feynman diagrams contributing to W boson production at $\mathcal{O}(\alpha^3)$ (Φ^+: Higgs–ghost field, u^+, u^γ: Faddeev-Popov-ghost fields; the non-photonic contribution to the W self energy insertion is symbolized by the shaded loop). An explicit representation of the non-photonic contribution to the W self energy insertion can be found in Ref. [26].

state, final state and interference corrections. The soft photon region is defined by requiring that the photon energy in the parton center of mass frame, $\hat{E}_\gamma$, is $\hat{E}_\gamma < E_{cut} = \delta_s \sqrt{\hat{s}}/2$. In this phase space region, the soft photon approximation can be used to calculate the cross section, provided that δ_s is sufficiently small. The soft singularities are regularized by giving the photon a fictitious small mass. In the sum of the virtual and soft photon terms the unphysical photon mass dependence cancels, and the QED-like contributions are IR finite.

The IR finite remainder of the virtual photonic corrections and the pure weak one-loop corrections of Fig. 1 can be combined to separately gauge invariant modified weak contributions to the W boson production and decay processes. Both the QED-like and the modified weak contributions are expressed in terms of form factors, F^a_{QED} and $\tilde{F}^a_{weak}$, which multiply the Born cross section [18]. The superscript a in the form factors denotes the initial state, final state or interference contributions.

The complete $\mathcal{O}(\alpha^3)$ parton level cross section of resonant W production via the Drell-Yan mechanism $q_i \overline{q_{i'}} \to \ell^+ \nu(\gamma)$ can then be written as follows [18]:

$$d\hat{\sigma}^{(0+1)} = d\hat{\sigma}^{(0)}[1 + 2\mathcal{R}e(\tilde{F}^{initial}_{weak} + \tilde{F}^{final}_{weak})(M_W^2)] + \sum_{\substack{a=initial,final,\\ interf.}} [d\hat{\sigma}^{(0)} F^a_{QED}(\hat{s},\hat{t}) + d\hat{\sigma}^a_{2\to 3}], \quad (1)$$

where the Born cross section, $d\hat{\sigma}^{(0)}$, is of the Breit-Wigner form and $\hat{s}$ and $\hat{t}$ are the usual Mandelstam variables in the parton center of mass frame. The modified weak contributions have to be evaluated at $\hat{s} = M_W^2$ [18]. Explicit expressions for the form factors $F^a_{QED}, \tilde{F}^a_{weak}$ are given in Ref. [18]. The IR finite contribution $d\hat{\sigma}^a_{2\to 3}$ describes real photon radiation with $\hat{E}_\gamma > E_{cut}$.

Additional singularities occur when the photon is collinear with one of the charged fermions. These collinear singularities are regularized by retaining finite fermion masses. Thus, both $d\hat{\sigma}^a_{2\to 3}$ and F^a_{QED} ($a = initial,\ final$) contain large mass singular logarithms which have to be treated with special care. In the case of final state photon radiation, the mass singular logarithms cancel when inclusive observables are considered [Kinoshita-Lee-Nauenberg (KLN) theorem [27]]. For exclusive quantities, however, these logarithms can result in large corrections, and it may be necessary to perform a resummation of the soft and/or collinear photon emission terms. To increase the numerical stability of the inclusive calculation, it is advantageous to extract the collinear part from $d\hat{\sigma}^{final}_{2\to 3}$ and perform the cancellation of the mass singular logarithms analytically. The reduced $2 \to 3$ contribution, i.e., the real photon contribution away from the soft and collinear region, can be evaluated numerically using standard Monte Carlo techniques.

For initial state photonic corrections, the mass singular logarithms always survive. These logarithmic terms are equivalent to the $1/\epsilon$ singularity encountered in dimensional regularization ($D = 4 - 2\epsilon$ is the number of dimensions) with massless quarks. They are universal to all orders in perturbation theory, and can therefore be canceled by universal collinear counter terms generated by ''renormalizing'' the parton distribution functions (PDF's), in complete analogy to gluon emission in QCD.[2] In addition to the collinear counterterms, finite terms can be absorbed into the PDF's, introducing a QED factorization scheme dependence. We have carried out our calculation in the QED DIS and QED $\overline{\rm MS}$ scheme. The extraction of the collinear part from $d\hat{\sigma}^a_{2\to 3}$ and the renormalization of the PDF's are described in Secs. II A and II B, respectively. In Sec. II C we provide explicit expressions for the $\mathcal{O}(\alpha^3)$ cross section for W production in hadronic collisions in the QED DIS and QED $\overline{\rm MS}$ scheme, and study the dependence of the $\mathcal{O}(\alpha^3)$ cross section on the theoretical cutoff parameters which define the soft and collinear regions.

A. The extraction of collinear singularities from $d\hat{\sigma}^a_{2\to 3}$

The contribution of real photon emission to the $\mathcal{O}(\alpha^3)$ cross section for W production in hadronic collisions is given by

[2]Alternatively, these logarithmic terms can be retained in the calculation. They would lead to large corrections, but then also to large changes in the input PDF's.

$$d\hat{\sigma}_{real} = dP_{2\to 3} \overline{\sum} |\mathcal{M}_{BR}|^2, \tag{2}$$

where $dP_{2\to 3}$ is the product of the three particle phase space element and the flux factor,

$$dP_{2\to 3} = \frac{1}{2\hat{s}} \frac{1}{(2\pi)^5} \frac{d^3p_f d^3p_{f'} d^3k}{8p_f^0 p_{f'}^0 k^0} \times \delta(p_i + p_{i'} - p_f - p_{f'} - k), \tag{3}$$

and the Bremsstrahlung matrix element $\mathcal{M}_{BR}$ is given by

$$\mathcal{M}_{BR} = i \frac{\pi\alpha}{2s_w^2} \sqrt{4\pi\alpha} \left\{ \frac{1}{\hat{s} - M_W^2} \overline{u}_f G^\rho_{\mu,f} \times (1-\gamma_5) v_{f'} \overline{v}_{i'} \gamma^\mu (1-\gamma_5) u_i - \frac{1}{\hat{s} - M_W^2 - 2kq} \overline{u}_f \gamma_\mu (1-\gamma_5) \times v_{f'} \overline{v}_{i'} G_i^{\mu\rho} (1-\gamma_5) u_i \right\} \epsilon_\rho^*(k). \tag{4}$$

In Eq. (4), $s_w^2 = \sin^2\theta_W$, where θ_W is the weak mixing angle, ϵ_ρ denotes the photon polarization vector, and

$$G_f^{\mu\rho} = Q_f \frac{(p_f^\rho + \gamma^\rho \not{k}/2)\gamma^\mu}{kp_f} - Q_{f'} \frac{\gamma^\mu (p_{f'}^\rho + \not{k}\gamma^\rho/2)}{kp_{f'}} - \frac{\gamma^\mu q^\rho + k^\mu \gamma^\rho - g^{\mu\rho}\not{k}}{kq},$$

$$G_i^{\mu\rho} = Q_i \frac{\gamma^\mu (p_i^\rho - \not{k}\gamma^\rho/2)}{kp_i} - Q_{i'} \frac{(p_{i'}^\rho - \gamma^\rho \not{k}/2)\gamma^\mu}{kp_{i'}} - \frac{\gamma^\mu q^\rho - k^\mu \gamma^\rho + g^{\mu\rho}\not{k}}{kq}. \tag{5}$$

Q_a $(a = i, i', f, f')$ denotes the electric charge in units of the proton charge, e. The initial and final state currents are separately conserved: $k_\rho G_f^{\mu\rho} = (Q_f - Q_{f'} - 1)\gamma^\mu = 0$ and $k_\rho G_i^{\mu\rho} = (Q_i - Q_{i'} - 1)\gamma^\mu = 0$.

$d\hat{\sigma}_{real}$ can be decomposed into soft and hard initial state, final state and interference terms:

$$d\hat{\sigma}_{real} = \sum_{\substack{a = initial, final, \\ interf.}} (d\hat{\sigma}^a_{soft} + d\hat{\sigma}^a_{2\to 3}). \tag{6}$$

Here, $d\hat{\sigma}^a_{soft}$ are the soft photon contributions ($\hat{E}_\gamma < E_{cut}$) and, as explained before, are included in the QED-like form factors F^a_{QED}.

The initial and final state hard photon contributions, $d\hat{\sigma}^{initial}_{2\to 3}$ and $d\hat{\sigma}^{final}_{2\to 3}$, contain mass singular logarithmic terms, whereas the interference contribution, $d\hat{\sigma}^{interf}_{2\to 3}$, does not. In order to extract the mass singular terms from $d\hat{\sigma}^{initial}_{2\to 3}$ and $d\hat{\sigma}^{final}_{2\to 3}$, we define a collinear region by requiring that

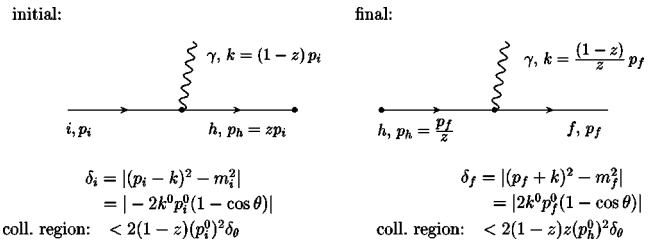

FIG. 2. The splitting of the initial and final state fermions $i(p_i) \to h(p_h) + \gamma$ and $h(p_h) \to f(p_f) + \gamma$ in the collinear region. The hard momentum p_h represents the amount of the parent momentum $p_{i,f}$ after (before) the emission of a collinear photon.

$$\cos\theta > 1 - \delta_\theta, \tag{7}$$

where θ is the angle between the charged fermion and the emitted photon in the parton center of mass frame. $d\hat{\sigma}^a_{2\to 3}$ can be decomposed into a finite contribution away from the soft and collinear singularity, $d\hat{\sigma}^{a,finite}_{2\to 3}$, which will be evaluated numerically, and a collinear part $d\hat{\sigma}^a_{coll}$, for which the integration over the singular phase space region can be performed analytically,

$$d\hat{\sigma}^a_{2\to 3} = d\hat{\sigma}^a_{coll} + d\hat{\sigma}^{a,finite}_{2\to 3} \quad a = \text{initial, final.} \tag{8}$$

In the following we calculate $d\hat{\sigma}^a_{coll}$ explicitly for both initial and final state photon radiation.

In the collinear region, $dP_{2\to 3}$ factorizes into a two particle and a collinear part (see Fig. 2 for notation)

initial state:

$$dP_{2\to 3}(i + i' \to f + f' + \gamma) \to dP_{2\to 2}(h + i' \to f + f') \frac{z d^3k}{2(2\pi)^3 k^0} = -dP_{2\to 2} \frac{z dz d\delta_i}{16\pi^2} \tag{9}$$

final state:

$$dP_{2\to 3}(i + i' \to f + f' + \gamma) \to dP_{2\to 2}(i + i' \to h + f') \frac{z^2 d^3k}{2(2\pi)^3 k^0} = -dP_{2\to 2} \frac{dz d\delta_f}{16\pi^2}, \tag{10}$$

where we have used

$$d^3k = 2\pi (k^0)^2 dk^0 d\cos\theta,$$

$$d\delta_{i,f} = 2k^0 p^0_{i,f} d\cos\theta; \quad dk^0 = -p_i^0 dz = -\frac{1}{z^2} p_f^0 dz. \tag{11}$$

Using the leading pole approximation, the squared matrix element for initial and final state photon emission [see Eq. (4)] factorizes into the leading-order squared matrix element,

$|\mathcal{M}^{(0)}|^2$, and a collinear factor, $c_{i\to h\gamma}$ or $c_{f\gamma\to h}$, provided the parameter δ_θ is sufficiently small:

$$\overline{\sum}|\mathcal{M}_{BR}^{initial}|^2(i+i'\to f+f'+\gamma)$$
$$\to\overline{\sum}|\mathcal{M}^{(0)}|^2(h+i'\to f+f')c_{i\to h\gamma},$$
$$\overline{\sum}|\mathcal{M}_{BR}^{final}|^2(i+i'\to f+f'+\gamma)$$
$$\to\overline{\sum}|\mathcal{M}^{(0)}|^2(i+i'\to h+f')c_{f\gamma\to h}. \quad (12)$$

Here

$$c_{i\to h\gamma}=8\pi^2\frac{\alpha}{\pi}Q_i^2\frac{1}{\delta_i}\left[\frac{1+z^2}{z(1-z)}-\frac{2m_i^2}{\delta_i}\right],$$
$$c_{f\gamma\to h}=8\pi^2\frac{\alpha}{\pi}Q_f^2\frac{1}{\delta_f}\left[\frac{1+z^2}{1-z}-\frac{2m_f^2}{\delta_f}\right], \quad (13)$$

and m_i (m_f) is the mass of the initial (final) state fermion which emits the photon. Combining Eqs. (9), (10) and (12), the hard photon contribution in the collinear limit reads (see also Ref. [28])

initial state:

$$d\hat{\sigma}_{coll}^{initial}=\int_0^{1-\delta_s}dz\Bigg\{d\hat{\sigma}^{(0)}(h+i'\to f+f')\times\int_{(1-z)m_i^2}^{2(1-z)(p_i^0)^2\delta_\theta}d\delta_i\,\frac{z}{16\pi^2}\,c_{i\to h\gamma}+(i\leftrightarrow i')\Bigg\}$$
$$=\int_0^{1-\delta_s}dz\Bigg\{d\hat{\sigma}^{(0)}\frac{\alpha}{2\pi}Q_i^2\Bigg[\frac{1+z^2}{1-z}\ln\left(\frac{\hat{s}_{i'h}}{m_i^2}\frac{\delta_\theta}{2}\frac{1}{z}\right)-\frac{2z}{1-z}\Bigg]+(i\leftrightarrow i')\Bigg\}, \quad (14)$$

final state:

$$d\hat{\sigma}_{coll}^{final}=\int_0^{1-\delta_s}dz\Bigg\{d\hat{\sigma}^{(0)}(i+i'\to h+f')\times\int_{(1-z)/zm_f^2}^{2z(1-z)(p_h^0)^2\delta_\theta}d\delta_f\,\frac{1}{16\pi^2}\,c_{f\gamma\to h}+(f\leftrightarrow f')\Bigg\}$$
$$=\int_0^{1-\delta_s}dz\Bigg\{d\hat{\sigma}^{(0)}\frac{\alpha}{2\pi}Q_f^2\Bigg[\frac{1+z^2}{1-z}\ln\left(\frac{\hat{s}_{f'h}}{m_f^2}\frac{\delta_\theta}{2}z^2\right)-\frac{2z}{1-z}\Bigg]+(f\leftrightarrow f')\Bigg\}, \quad (15)$$

with $\hat{s}_{i'h;f'h}=(p_h+p_{i';f'})^2$. In order to avoid double counting in the soft region, the upper limit in the z integration has to be reduced from $z=1$ to $z=1-\delta_s$ in Eqs. (14) and (15).

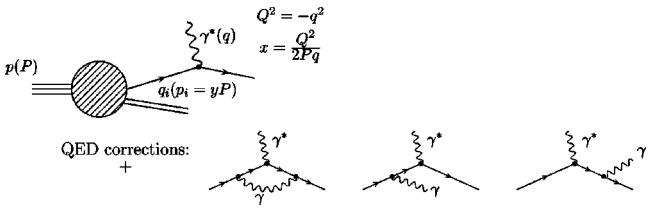

FIG. 3. The QED one-loop corrections in deep inelastic lepton-nucleon scattering.

B. Mass factorization: QED DIS and $\overline{\text{MS}}$ scheme

The mass singular logarithmic terms of Eq. (14) can be absorbed by the counter terms to the PDF's. In addition to the singular terms, finite $\mathcal{O}(\alpha)$ terms can be absorbed into the PDF's. At next-to-leading order (NLO) in QED, the parton distribution functions therefore depend on the QED factorization scheme used. In this subsection, we derive the NLO PDF's in the QED DIS and the QED $\overline{\text{MS}}$ scheme.

In order to derive the parton distribution functions at next-to-leading order in QED, one must calculate the virtual and real photon contribution to the square of the parton electromagnetic current, integrated over the phase space of the final state partons, $\hat{W}_{\mu\nu}^i$. The contributing Feynman diagrams are shown in Fig. 3. The tensor $\hat{W}_{\mu\nu}^i$ is related to the structure function $F_2(x,Q^2)$ by (see Fig. 3 for notation)

$$F_2(x,Q^2)=\frac{x}{4\pi}\sum_i\int_x^1\frac{dy}{y}\,q_i(y)\times\left[-g^{\mu\nu}+\frac{12x^2}{Q^2y^2}P^\mu P^\nu\right]\hat{W}_{\mu\nu}^i, \quad (16)$$

where the sum is taken over all contributing quark flavors, and the $q_i(y)$ are the unrenormalized quark distribution functions. Since it involves an additional power of α, we do not take into account the photon content of the proton in our calculation.

In the physical (DIS) scheme [29] the ''renormalized'' quark distribution functions are defined by requiring that $F_2(x,Q^2)$ is given by the sum of the quark distributions to all orders in perturbation theory

$$F_2(x,Q^2)=x\sum_i Q_i^2[q_i^{DIS}(x,Q^2)+\overline{q}_i^{DIS}(x,Q^2)], \quad (17)$$

where the QED factorization scale has been set equal to Q. The $\mathcal{O}(\alpha)$ structure function $F_2(x,Q^2)$ can be obtained from the corresponding $\mathcal{O}(\alpha_s)$ QCD structure function [30] by the replacement

$$\frac{\alpha_s}{\pi}\frac{4}{3}\to\frac{\alpha}{\pi}Q_i^2. \quad (18)$$

For massive fermions one finds in the limit $Q^2\gg m_i^2$ ($z=x/y$):

$$F_2(x,Q^2)=x\sum_i Q_i^2\Bigg(\int_x^1 \frac{dz}{z}\, q_i\Big(\frac{x}{z}\Big)\Bigg\{\delta(1-z)+\frac{\alpha}{\pi}Q_i^2\Bigg[\Big(2\ln\delta_s+\frac{3}{2}\Big)\ln\Big(\frac{Q^2}{m_i^2}\Big)\delta(1-z)+\frac{1+z^2}{1-z}\ln\Big(\frac{Q^2}{m_i^2}\frac{1}{(1-z)z}\Big)$$
$$\times\theta(1-\delta_s-z)-\Big[\ln^2\delta_s+\frac{7}{2}\ln\delta_s+\frac{5}{2}+\frac{\pi^2}{3}\Big]\delta(1-z)+\Big[\frac{1}{2}\frac{1-8z}{1-z}+3z\Big]\theta(1-\delta_s-z)\Bigg]\Bigg\}\Bigg). \tag{19}$$

Using Eq. (19) it is then straightforward to calculate $q_i^{DIS}(x,Q^2)$ in terms of the unrenormalized quark distribution functions $q_i(x)$ (see below). The relation between $F_2(x,Q^2)$ and the quark distribution functions in the $\overline{\rm MS}$ scheme [31] is given by

$$F_2(x,Q^2)=x\sum_i Q_i^2[q_i^{\overline{MS}}(x,Q^2)+\overline{q}_i^{\overline{MS}}(x,Q^2)]+x\sum_i Q_i^2\int_x^1\frac{dy}{y}\,[q_i^{\overline{MS}}(y,Q^2)+\overline{q}_i^{\overline{MS}}(y,Q^2)]\,\frac{\alpha}{\pi}\,c_i\Big(\frac{x}{y}\Big), \tag{20}$$

with [32]

$$c_i(z)=\frac{1}{2}Q_i^2\Bigg\{\Big[\ln^2\delta_s-\frac{3}{2}\ln\delta_s-\frac{9}{2}+\frac{\pi^2}{3}\Big]\delta(1-z)+\Big[\frac{1+z^2}{1-z}\ln\frac{1-z}{z}-\frac{3}{2}\frac{1}{1-z}+2z+3\Big]\theta(1-\delta_s-z)\Bigg\}. \tag{21}$$

$c_i(z)$ represents the finite part of the QED $O(\alpha)$ corrections to deep inelastic scattering after removing the singularities according to the $\overline{\rm MS}$ prescription. The $\overline{\rm MS}$ scheme is defined in the framework of dimensional regularization but Eq. (20) can also be used for its definition. To obtain the renormalized quark distribution functions, $q_i^{\overline{MS}}(x,Q^2)$, when finite quark masses are used as regulators, we make use of the relation

$$q_i^{\overline{MS}}(x,Q^2)+\int_x^1\frac{dy}{y}\,q_i^{\overline{MS}}(y,Q^2)\,\frac{\alpha}{\pi}\,c_i\Big(\frac{x}{y}\Big)=q_i^{DIS}(x,Q^2), \tag{22}$$

which follows from Eqs. (17) and (20).

The final expression for the scheme dependent renormalized quark distribution function in NLO QED is

$$q_i(x,Q^2)=q_i(x)\Bigg[1+\frac{\alpha}{\pi}Q_i^2\Bigg\{1-\ln\delta_s-\ln^2\delta_s+\Big(\ln\delta_s+\frac{3}{4}\Big)\ln\Big(\frac{Q^2}{m_i^2}\Big)-\frac{1}{4}\lambda_{FC}f_{v+s}\Bigg\}\Bigg]$$
$$+\int_x^{1-\delta_s}\frac{dz}{z}\,q_i\Big(\frac{x}{z}\Big)\,\frac{\alpha}{2\pi}\,Q_i^2\Bigg\{\frac{1+z^2}{1-z}\ln\Big(\frac{Q^2}{m_i^2}\frac{1}{(1-z)^2}\Big)-\frac{1+z^2}{1-z}+\lambda_{FC}f_c\Bigg\}, \tag{23}$$

with

$$f_{v+s}=9+\frac{2\pi^2}{3}+3\ln\delta_s-2\ln^2\delta_s, \tag{24}$$

and

$$f_c=\frac{1+z^2}{1-z}\ln\Big(\frac{1-z}{z}\Big)-\frac{3}{2}\frac{1}{1-z}+2z+3. \tag{25}$$

The QED DIS ($\overline{\rm MS}$) scheme corresponds to $\lambda_{FC}=1$ ($\lambda_{FC}=0$).

C. The cross section for $p\overset{(-)}{p}\to W(\gamma)\to\ell\nu(\gamma)$

The differential cross section for $p\overset{(-)}{p}\to W(\gamma)\to\ell\nu(\gamma)$ is obtained by convoluting the parton cross section of Eq. (1) with $q_i(x)$, and subsequently replacing the unrenormalized quark distribution functions by $q_i(x,Q^2)$, using Eq. (23). The initial state QED-like contribution $d\hat{\sigma}^{(0)}F_{QED}^{initial}$ and the collinear part $d\hat{\sigma}_{coll}^{initial}$, including the effect of mass factorization, can be grouped into a single $2\to2$ contribution:

$$d\sigma_{2\to 2}^{initial}=\sum_{i,i'}\int dx_1 dx_2[q_i(x_1,Q^2)\overline{q}_{i'}(x_2,Q^2)d\hat{\sigma}^{(0)}+(1\leftrightarrow 2)]$$
$$\times\frac{\alpha}{\pi}\left\{(Q_i^2+Q_{i'}^2)\left[\left(\ln\,\delta_s+\frac{3}{4}\right)\ln\left(\frac{\hat{s}}{Q^2}\right)+\frac{\pi^2}{6}-2+\ln^2\,\delta_s+\frac{1}{4}\lambda_{FC}f_{v+s}\right]-\ln\,\delta_s+\frac{3}{2}+\frac{\pi^2}{24}\right\}$$
$$+\sum_{i,i'}\int dx_1 dx_2\left\{\int_{x_2}^{1-\delta_s}\frac{dz}{z}\left[Q_i^2 q_i\left(\frac{x_2}{z},Q^2\right)\overline{q}_{i'}(x_1,Q^2)+Q_{i'}^2 q_i(x_1,Q^2)\overline{q}_{i'}\left(\frac{x_2}{z},Q^2\right)\right]d\hat{\sigma}^{(0)}\,\frac{\alpha}{2\pi}\right.$$
$$\left.\times\left[\frac{1+z^2}{1-z}\ln\left(\frac{\hat{s}}{Q^2}\,\frac{(1-z)^2}{z}\,\frac{\delta_\theta}{2}\right)+1-z-\lambda_{FC}f_c\right]+(1\leftrightarrow 2)\right\}. \tag{26}$$

As expected, the mass singular logarithms cancel completely. x_1 and x_2 in Eq. (26) are the momentum fractions of the parent hadrons carried by the partons.

In order to treat the $\mathcal{O}(\alpha)$ initial state QED-like corrections to W production in hadronic collisions in a consistent way, QED corrections should be incorporated in the global fitting of the PDF's using the same factorization scheme which has been employed to calculate the cross section. Current fits [33] to the PDF's do not include QED corrections. A study of the effect of QED corrections on the evolution of the parton distribution functions indicates [19] that the modification of the PDF's is small. We have not attempted to include QED corrections to the PDF evolution in the calculation presented here. The missing QED corrections to the PDF introduce an uncertainty which, however, is likely to be smaller than the present uncertainties on the parton distribution functions.

The squared matrix elements for different QED factorization schemes differ by the finite $\mathcal{O}(\alpha)$ terms which are absorbed into the PDF's in addition to the singular terms. In the QED DIS scheme, the contribution of the QED-like initial state corrections to the cross section is about 8% smaller than in the QED $\overline{\rm MS}$ scheme. The factorization scheme dependence is expected to be reduced when the $\mathcal{O}(\alpha)$ QED corrections to the PDF are included. In the following, for the numerical evaluation of $d\sigma_{2\to 2}^{initial}$, we use the QED $\overline{\rm MS}$ scheme.

The final state $2\to 2$ contribution can be obtained directly from the form factor F_{QED}^{final} of Ref. [18] with $Q_{f=\nu}=0$ and $Q_{f'=\ell}=-1$:

$$d\sigma_{2\to 2}^{final}=\sum_{i,i'}\int dx_1 dx_2[q_i(x_1,Q^2)$$
$$\times\overline{q}_{i'}(x_2,Q^2)d\hat{\sigma}^{(0)}+(1\leftrightarrow 2)]$$
$$\times\frac{\alpha}{\pi}\left\{\left(\ln\,\delta_s+\frac{3}{4}\right)\ln\left(\frac{\hat{s}}{m_\ell^2}\right)\right.$$
$$\left.-2\ln\,\delta_s+\frac{1}{2}+\frac{5\pi^2}{24}\right\}. \tag{27}$$

In sufficiently inclusive observables the mass singular logarithmic terms cancel in the sum of $d\sigma_{2\to 2}^{final}$ and $d\sigma_{2\to 3}^{final}$.

The approximation used so far in modeling the EW radiative corrections to W boson production at the Tevatron [13,14] ignores all weak, interference and initial state photonic corrections, and differs from our calculation in the treatment of the final state virtual and soft photon contribution. At the parton level, the difference between Eq. (27) and the $2\to 2$ contribution to the differential cross section in the approximate calculation, is given by

$$\Delta\hat{\sigma}^{final}=d\hat{\sigma}^{(0)}\,\frac{\alpha}{2\pi}\left\{\left[\ln\left(\frac{m_\ell^2}{M_W^2}\,\delta_s^2\right)+\frac{7}{2}\right]\right.$$
$$\left.\times\ln\left(\frac{\hat{s}}{M_W^2}\right)+\frac{3\pi^2}{4}-1\right\}. \tag{28}$$

In Sec. III A we demonstrate that the difference has a non-negligible effect on the shape of the transverse mass distribution.

Experimentally, photons which are collinear with muons can be identified without problems: photons deposit energy in the electromagnetic calorimeter, whereas muons are identified by hits in the muon chambers. For muons in the final state, therefore, one has to retain full information on the particle momentum four vectors. In the electron case, on the other hand, the finite resolution of detectors makes it difficult to discriminate between electrons and photons with a small opening angle, and the electron and photon four-momentum vectors are recombined to an effective electron four-momentum vector if their separation $\Delta R_{e\gamma}$ in the azimuthal angle–pseudorapidity plane is smaller than a critical value R_c. If the lepton and photon four-momentum vectors are not resolved in the collinear region, the collinear singularities from the hard photon contribution can be extracted as described in Sec. II A, and the integration over the momentum fraction z in Eq. (15) can be performed analytically. The parameter δ_θ has to be chosen sufficiently small to ensure that $\Delta R_{e\gamma}<R_c$ over the entire region where the analytic integration is carried out. For small R_c one finds that δ_θ has to be less than

$$\delta_\theta^{\max}\approx\frac{R_c^2}{2\cosh^2(\eta^{\max}(e))}, \tag{29}$$

where $\eta^{\max}(e)$ is the maximum allowed pseudorapidity of the electron.

The procedure described above is part of the electron identification process used by the DØ Collaboration [16]. The Collider Detector at Fermilab (CDF) Collaboration uses a slightly different method where the electron and photon four-momentum vectors are combined if both particles traverse the same calorimeter cell. This modifies the expression for $\delta_\theta^{\max}$.

Once the integration over z has been performed analytically, the collinear contribution $d\hat{\sigma}_{coll}^{final}$ and the QED-like contribution $d\hat{\sigma}^{(0)}F_{QED}^{final}$ can be combined to cancel the mass singular logarithms explicitly, and one obtains for the final state $2\to2$ contribution

$$d\tilde{\sigma}_{2\to2}^{final}=\sum_{i,i'}\int dx_1dx_2[q_i(x_1,Q^2)\overline{q}_{i'}(x_2,Q^2)\times d\hat{\sigma}^{(0)}+(1\leftrightarrow2)]\frac{\alpha}{\pi}\left\{-\ln\,\delta_s+\frac{11}{4}-\frac{\pi^2}{8}-\left(\ln\,\delta_s+\frac{3}{4}\right)\ln\left(\frac{\delta_\theta}{2}\right)\right\}. \tag{30}$$

As described in Ref. [18], a part of the photonic interference terms together with the IR finite parts of the box diagrams in Fig. 1 can be absorbed into the modified weak contributions $\tilde{F}_{weak}^{initial,final}$ introduced earlier in this section. The $2\to2$ interference contribution is then given by

$$d\sigma_{2\to2}^{interf}=\sum_{i,i'}\int dx_1dx_2q_i(x_1,Q^2)\overline{q}_{i'}(x_2,Q^2)d\hat{\sigma}^{(0)}\times\frac{1}{2}\,\beta_{int}(\hat{s},\hat{t},\hat{u})\ln\left(\frac{\delta_s^2M_W^4}{(\hat{s}-M_W^2-\hat{s}\,\delta_s)^2+M_W^2\Gamma_W^2}\right)+(1\leftrightarrow2), \tag{31}$$

where Γ_W is the W width, and

$$\beta_{int}(\hat{s},\hat{t},\hat{u})=\frac{\alpha}{\pi}\left[Q_i\,\ln\left(\frac{\hat{u}^2}{\hat{s}^2}\right)-Q_{i'}\,\ln\left(\frac{\hat{t}^2}{\hat{s}^2}\right)+2\right]. \tag{32}$$

For $\hat{s}=M_W^2$, the $2\to2$ interference contribution is completely cancelled by the hard photon contribution $d\hat{\sigma}_{2\to3}^{interf}$ when the total inclusive cross section is calculated. Note that the $2\to2$ interference contribution exhibits only soft singularities.

The complete $\mathcal{O}(\alpha^3)$ cross section for $p\overset{(-)}{p}\to W(\gamma)\to\ell\nu(\gamma)$ can now be expressed as

$$d\sigma^{(0+1)}=\sum_{i,i'}\int dx_1dx_2[q_i(x_1,Q^2)\overline{q}_{i'}(x_2,Q^2)d\hat{\sigma}^{(0)}+(1\leftrightarrow2)][1+2\,\mathrm{Re}(\tilde{F}_{weak}^{initial}+\tilde{F}_{weak}^{final})(M_W^2)]+d\sigma_{2\to2}^{initial}+d\sigma_{2\to3}^{initial,finite}+d\sigma_{2\to2}^{interf}+d\sigma_{2\to3}^{interf}+d\sigma^{final} \tag{33}$$

with

$$d\sigma^{final}=d\sigma_{2\to2}^{final}+d\sigma_{2\to3}^{final}, \tag{34}$$

if the integration over z is performed numerically, and

$$d\sigma^{final}=d\tilde{\sigma}_{2\to2}^{final}+d\sigma_{2\to3}^{final,finite}, \tag{35}$$

if the z integration is done analytically. Here, $d\sigma_{2\to3}^{a,finite}$ ($a=initial,\ final$) are the reduced $2\to3$ contributions away from the soft and collinear region. The hard bremsstrahlung contribution has been compared numerically with the $p\overset{(-)}{p}\to\ell\nu\gamma$ cross section of Ref. [34]. The two calculations agree to better than 1%.

The end result of the calculation consists of two sets of weighted events corresponding to the $2\to2$ and $2\to3$ contributions. Each set depends on the parameters δ_s and δ_θ. The sum of the two contributions, however, must be independent of δ_s and δ_θ, as long as the two parameters are taken small enough so that the soft photon and the leading pole approximation are valid. In Figs. 4–6 we show the different contributions to the $p\overline{p}\to\ell^+\nu(\gamma)$ cross section at $\sqrt{s}=1.8$ TeV as a function of the two parameters. To compute the cross section, we use here and in all subsequent figures the Martin-Roberts-Stirling set A (MRSA) set of parton distribution functions [35], and take the QCD renormalization scale μ_{QCD} and the QED and QCD factorization scales, M_{QED} and M_{QCD}, to be $\mu_{QCD}^2=Q^2=M_{QED}^2=M_{QCD}^2=M_W^2$. The detector acceptance is simulated by imposing the following transverse momentum (p_T) and pseudorapidity (η) cuts:

$$p_T(\ell)>25\ \mathrm{GeV},\quad |\eta(\ell)|<1.2,\quad \ell=e,\mu, \tag{36}$$

$$\not{p}_T>25\ \mathrm{GeV}. \tag{37}$$

These cuts approximately model the acceptance cuts used by the CDF and DØ collaborations in their W mass analyses [15,16]. Uncertainties in the energy and momentum measurements of the charged leptons in the detector are simulated in the calculation by Gaussian smearing of the particle four-momentum vector with standard deviation σ which depends on the particle type and the detector. The numerical results presented here were calculated using σ values based on the specifications for the upgraded Run II DØ detector

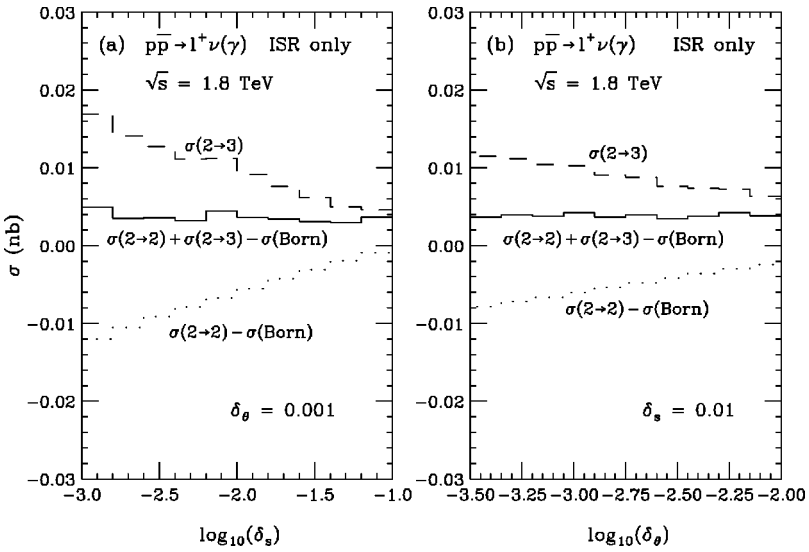

FIG. 4. The QED-like initial state corrections to the $p\bar{p}\to\ell^+\nu(\gamma)$, ($\ell=e,\mu$) cross section for $\sqrt{s}=1.8$ TeV as a function of (a) δ_s for $\delta_\theta=0.001$, and (b) δ_θ for $\delta_s=0.01$. Shown are $\sigma(2\to2)-\sigma(\text{Born})$, $\sigma(2\to3)$, and $\sigma(2\to2)+\sigma(2\to3)-\sigma(\text{Born})$. The cuts imposed are listed in Eqs. (36) and (37). The energy and momentum resolutions used are described in the text.

[36]. The results obtained using the target specifications for the CDF II detector [37] are similar. The SM parameters used in our numerical simulations are $M_W=80.3$ GeV, $M_Z=91.187$ GeV, $\alpha=\alpha(0)=1/137.036$, $G_\mu=1.166\times10^{-5}$ GeV^{-2}, $\Gamma_W=2.1$ GeV, and $m_{top}=175$ GeV. These values are consistent with recent measurements at LEP, SLAC Linear Collider (SLC) and the Tevatron [1].

Figure 4 displays the QED-like initial state (ISR) corrections to the cross section as a function of δ_s [Fig. 4(a)] and δ_θ [Fig. 4(b)]. In order to exhibit the independence of the cross section from the parameters δ_s and δ_θ more clearly, we have not included the Born cross section in the $2\to2$ contribution here as well as in Figs. 5 and 6. The QED-like ISR corrections to the cross section for electron and muon final states are virtually identical. While the separate $2\to2$ and $2\to3$ $\mathcal{O}(\alpha)$ contributions vary strongly with δ_s and δ_θ, the sum is independent of the two parameters within the accuracy of the Monte Carlo integration.

In Fig. 5, we show the QED-like final state (FSR) corrections to the $p\bar{p}\to\ell^+\nu(\gamma)$ cross section as a function of δ_s for electron and muon final states. Radiation of photons collinear with one of the leptons gives rise to terms proportional to $[\ln(\hat{s}/m_\ell^2)-2]\ln(\delta_s)$ [see Eq. (27)] in both the $2\to2$ and $2\to3$ contributions. As demonstrated in Fig. 5, these terms cancel and the total cross section is independent of δ_s. Due to the smaller mass of the electron, the variation of the $2\to2$ and $2\to3$ contributions with δ_s is more pronounced in the electron case.

In Figs. 4 and 5, we have not taken into account realistic lepton identification requirements, i.e., we have assumed that photons and leptons with arbitrary small opening angles can be discriminated. In a more realistic simulation, in addition to the lepton p_T, $\not{p}_T$ and pseudorapidity cuts, one imposes requirements on the separation of the charged lepton and the photon. These requirements differ slightly for the CDF and DØ detectors. In the following we adopt lepton identification criteria which are motivated by the DØ W mass [16] and W cross section [25] analyses; the numerical results obtained using the requirements imposed in the CDF W mass analysis [15] are similar. In order to study their impact on the size of

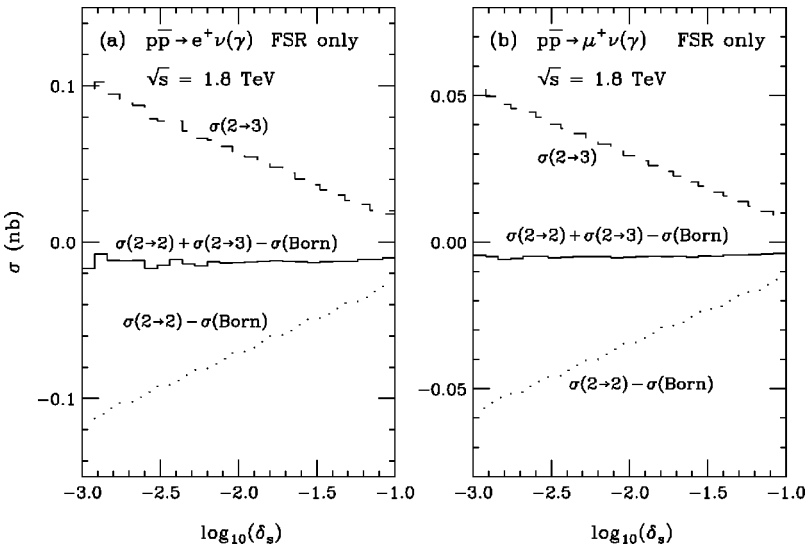

FIG. 5. The QED-like final state corrections to the cross section (a) $\sigma(p\bar{p}\to e^+\nu(\gamma))$ and (b) $\sigma(p\bar{p}\to\mu^+\nu(\gamma))$ for $\sqrt{s}=1.8$ TeV as a function of δ_s. Shown are $\sigma(2\to2)-\sigma(\text{Born})$, $\sigma(2\to3)$, and $\sigma(2\to2)+\sigma(2\to3)-\sigma(\text{Born})$. The cuts imposed are listed in Eqs. (36) and (37). The energy and momentum resolutions used are described in the text.

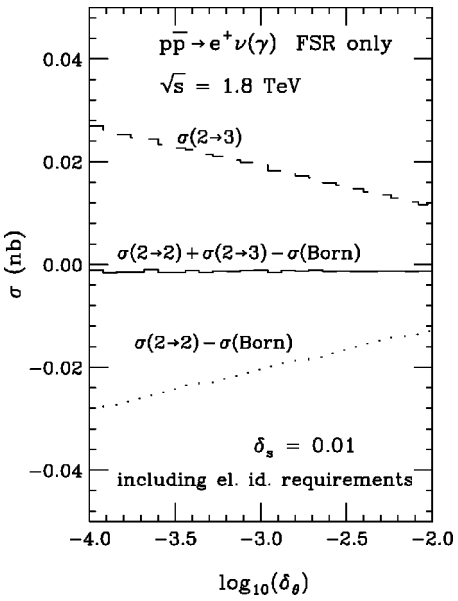

FIG. 6. The $p\bar{p}\to e^+\nu(\gamma)$ cross section for $\sqrt{s}=1.8$ TeV as a function of δ_θ for $\delta_s=0.01$ when electron identification requirements are taken into account and the mass singular terms are canceled analytically. Only QED-like final state radiative corrections are included. Shown are $\sigma(2\to2)-\sigma(\mathrm{Born})$, $\sigma(2\to3)$, and $\sigma(2\to2)+\sigma(2\to3)-\sigma(\mathrm{Born})$. The cuts and lepton identification requirements imposed are listed in Eqs. (36) and (37), and in Table I. The energy and momentum resolutions used are described in the text.

the EW radiative corrections, we will perform simulations both with and without the lepton identification requirements taken into account.

We shall use the following lepton identification requirements. For electrons, we require that the electron and photon momentum four-vectors are combined into an effective electron momentum four-vector if $\Delta R_{e\gamma}<0.2$. For $0.2<\Delta R_{e\gamma}<0.4$ events are rejected if $E_\gamma>0.15E_e$. Here E_γ (E_e) is the energy of the photon (electron) in the laboratory frame. For events with $0.2<\Delta R_{e\gamma}<0.3$ and $E_\gamma<0.15E_e$, the electron and photon momentum four vectors are again combined. Muons are identified by hits in the muon chambers and the requirement that the associated track is consistent with a minimum ionizing particle. This limits the photon energy for small muon-photon opening angles. For muons, we therefore require the energy of the photon to be $E_\gamma<2$ GeV for $\Delta R_{\mu\gamma}<0.2$, and $E_\gamma<6$ GeV for $0.2<\Delta R_{\mu\gamma}<0.6$. For future reference, we summarize the lepton identification requirements in Table I.

As noted before, when the electron and photon momentum four vectors are combined, it is possible to analytically cancel the mass singular terms in the QED-like $2\to2$ final state corrections. In this case, the QED-like final state $2\to2$ and $2\to3$ contributions depend on the collinear cutoff parameter δ_θ. Figure 6 displays the QED-like final state contribution to the $p\bar{p}\to e^+\nu(\gamma)$ cross section as a function of δ_θ when the electron identification requirements described above are taken into account. While the $2\to2$ and $2\to3$ contributions both exhibit a considerable dependence on δ_θ, their sum is independent of the parameter.

Similar to the QED-like initial and final state corrections, one can show that the sum of the $2\to2$ and $2\to3$ contributions of the QED-like initial—final state interference terms is independent of δ_s. The interference terms are typically of the same size as the initial state corrections. The modified weak contributions to the $\mathcal{O}(\alpha^3)$ cross section are trivially independent of δ_s and δ_θ. In the following, these parameters will be fixed to $\delta_s=10^{-2}$ and $\delta_\theta=10^{-3}$.

As stated before, we take the QCD renormalization scale μ_{QCD} and the QED and QCD factorization scales, M_{QED} and M_{QCD}, to be equal, $\mu_{QCD}=M_{QED}=M_{QCD}=Q$. The missing QED corrections to the PDF's create a dependence of the $\mathcal{O}(\alpha)$ initial state corrections on the scale Q which is stronger than that of the lowest order calculation. On the other hand, final state and initial–final state interference terms depend on Q only through the PDF's.

III. PHENOMENOLOGICAL RESULTS

We shall now discuss the phenomenological implications of the $\mathcal{O}(\alpha)$ electroweak corrections to W production at the Tevatron ($p\bar{p}$ collisions at $\sqrt{s}=1.8$ TeV). We first discuss the impact of electroweak corrections on observables used to measure M_W: the transverse mass distribution, the $p_T(\ell)$ distribution, and the W to Z transverse mass ratio. We then consider the W production cross section, the W to Z cross section ratio and the charge asymmetry of leptons in the W decay. Unless stated otherwise, we take into account the cuts of Eqs. (36) and (37) and effects from energy and momentum measurement uncertainties in the detector. We state explicitly when the lepton identification requirements listed in Table I are included.

A. Electroweak corrections to the M_T and $p_T(\ell)$ distributions, and the W to Z transverse mass ratio

Since the detectors at the Fermilab Tevatron collider cannot directly detect the neutrinos produced in the leptonic W boson decays, $W\to\ell\nu$, and cannot measure the longitudinal component of the recoil momentum, there is insufficient in-

TABLE I. Summary of lepton identification requirements.

Electrons	Muons
Combine e and γ momentum four vectors if	Reject events with $E_\gamma>2$ GeV
$\Delta R_{e\gamma}<0.2$ and if $E_\gamma<0.15E_e$ for $0.2<\Delta R_{e\gamma}<0.3$	for $\Delta R_{\mu\gamma}<0.2$
Reject events with $E_\gamma>0.15E_e$	Reject events with $E_\gamma>6$ GeV
for $0.2<\Delta R_{e\gamma}<0.4$	for $0.2<\Delta R_{\mu\gamma}<0.6$

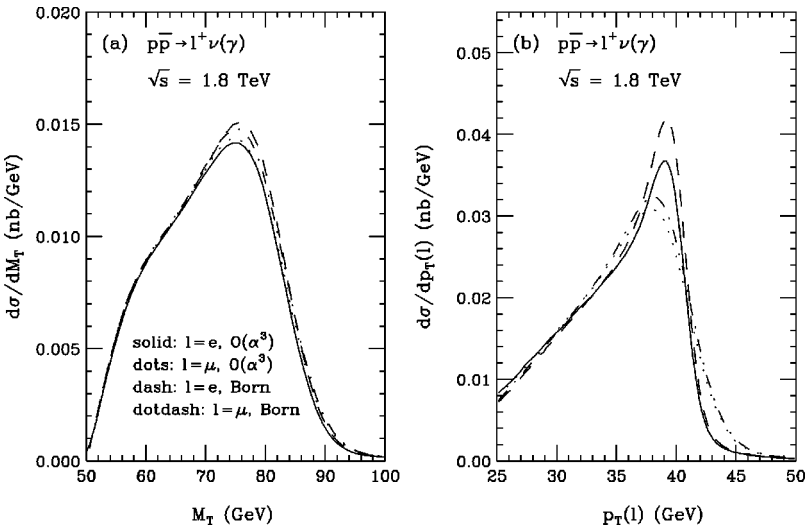

FIG. 7. Differential cross sections for $p\bar{p} \to \ell^+\nu(\gamma)$ at $\sqrt{s}=1.8$ TeV. Shown in part (a) is the transverse mass distribution. Part (b) displays the lepton transverse momentum spectrum. The solid (dotted) lines show the distributions for electron (muon) final states including $\mathcal{O}(\alpha)$ electroweak corrections. The dashed (dot-dashed) line gives the $e^+\nu$ ($\mu^+\nu$) Born cross section. The cuts imposed are listed in Eqs. (36) and (37). The energy and momentum resolutions used are described in Sec. II C. The lepton identification requirements of Table I are not taken into account here.

formation to reconstruct the invariant mass of the W boson. Instead, the transverse mass distribution of the final state lepton pair, or the transverse momentum distribution of the charged lepton are used [16] to extract M_W. The transverse mass is defined by

$$M_T = \sqrt{2 p_T(\ell) p_T(\nu)(1-\cos\phi^{\ell\nu})}, \tag{38}$$

where $p_T(\ell)$ and $p_T(\nu)$ are the transverse momentum of the lepton and the neutrino, and $\phi^{\ell\nu}$ is the angle between the charged lepton and the neutrino in the transverse plane. The neutrino transverse momentum is identified with the missing transverse momentum, $\not{p}_T$, in the event. Recently, it has been pointed out that the ratio of W to Z observables can also be used to measure the W mass [23]. This method has been applied to the W to Z transverse mass ratio by the DØ collaboration [24]. The advantages and disadvantages of the observables used to extract M_W are discussed in Ref. [6].

The $\mathcal{O}(\alpha^3)$ M_T distribution for $e^+\nu(\gamma)$ (solid) and $\mu^+\nu(\gamma)$ (dots) production is shown in Fig. 7(a) together with the lowest-order predictions (dashed and dot-dashed curves). In Fig. 7(b), we show the $\mathcal{O}(\alpha^3)$ and Born $p_T(\ell)$ spectrum. The flavor specific lepton identification requirements of Table I are not taken into account here. Electroweak corrections decrease the cross section at the peak of the M_T ($p_T(\ell)$) distribution by about 12% (17%) in the electron, and by about 6% (7%) in the muon case. Photon radiation from the charged lepton lowers the $\ell\nu$ invariant mass. Events from the Jacobian peak regions in the M_T and $p_T(\ell)$ distributions therefore are shifted on average to lower values of the transverse mass and transverse momentum. Due to the $\ln(\hat{s}/m_\ell^2)$ term, the effect of the corrections is larger in the electron case. The Jacobian peak of the p_T distribution is broader and less pronounced in the muon case, due to the energy and momentum resolution which is significantly worse for muons than for electrons. In the M_T distribution, the effect of the $\not{p}_T$ resolution dominates, and the difference in the distribution between electrons and muons is small. The M_T and $p_T(\ell)$ distributions for $\ell^-\nu(\gamma)$ production are identical to those for the $\ell^+\nu(\gamma)$ channel in $p\bar{p}$ collisions. In the remainder of this subsection we therefore only consider the $\ell^+\nu(\gamma)$ final state.

The various individual contributions to the EW $\mathcal{O}(\alpha)$ corrections on the M_T distribution are shown in Fig. 8. The

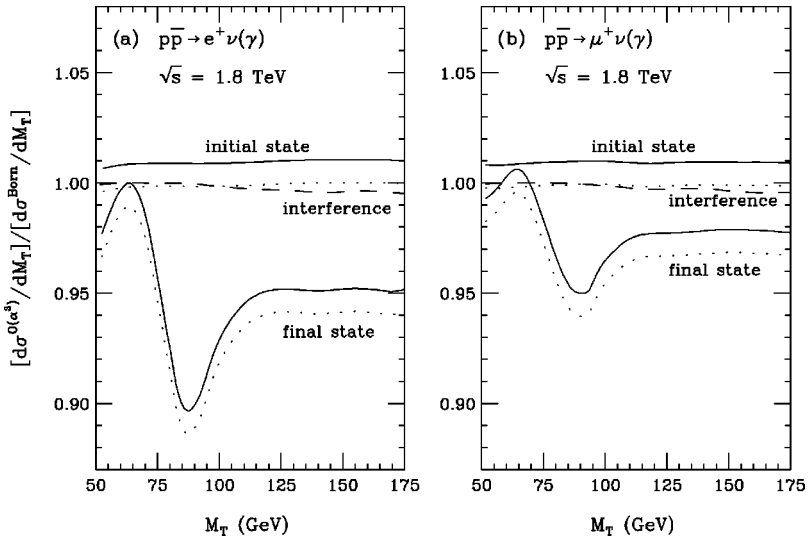

FIG. 8. Ratio of the $\mathcal{O}(\alpha^3)$ and lowest order cross sections as a function of the transverse mass for (a) $p\bar{p} \to e^+\nu(\gamma)$ and (b) $p\bar{p} \to \mu^+\nu(\gamma)$ at $\sqrt{s}=1.8$ TeV for various individual contributions. The upper (lower) solid lines show the result for the QED-like initial (final) state corrections. The upper (lower) dotted lines give the cross section ratios if both the QED-like and modified weak initial (final) state corrections are included. The dashed lines display the result if only the initial–final state interference contributions are included. The cuts imposed are listed in Eqs. (36) and (37). The energy and momentum resolutions used are described in Sec. II C. The lepton identification requirements of Table I are not taken into account here.

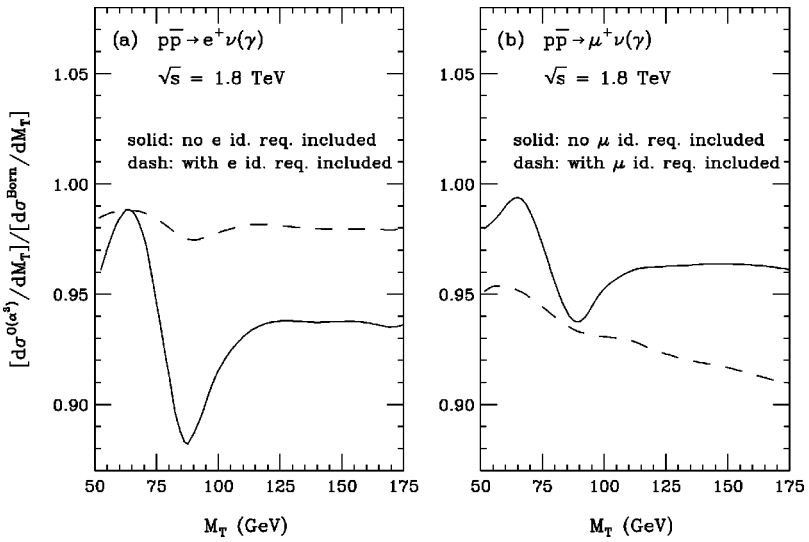

FIG. 9. Ratio of the full $\mathcal{O}(\alpha^3)$ and lowest order differential cross sections as a function of the transverse mass for (a) $p\bar{p} \to e^+\nu(\gamma)$ and (b) $p\bar{p} \to \mu^+\nu(\gamma)$ at $\sqrt{s} = 1.8$ TeV. The dashed (solid) lines show the result with (without) the lepton identification requirements of Table I taken into account. The cuts imposed are listed in Eqs. (36) and (37). The energy and momentum resolutions used are described in Sec. II C.

initial state QED-like contribution uniformly increases the cross section by about 1% for electron [Fig. 8(a)] and muon [Fig. 8(b)] final states. It is largely canceled by the modified weak initial state contribution. The interference contribution is very small. It decreases the cross section by about 0.01% for transverse masses below M_W, and by up to 0.5% for $M_T > M_W$. The final state QED-like contribution significantly changes the shape of the transverse mass distribution and reaches its maximum effect in the region of the Jacobian peak, $M_T \approx M_W$. As for the initial state, the modified weak final state contribution reduces the cross section by about 1%, and has no effect on the shape of the transverse mass distribution. For $M_T > 125$ GeV, the QED-like final state corrections uniformly reduce the differential cross section by about 5% in the electron case, and by about 2% in the muon case. Without taking the lepton identification requirements of Table I into account, the full $\mathcal{O}(\alpha)$ electroweak radiative corrections to the M_T distribution are very well approximated by the sum of the QED-like and modified weak final state corrections.

It should be noted that the differential cross section ratio shown in Fig. 8 becomes ill defined in the threshold region $M_T \approx p_T^{cut}(\ell) + \not{p}_T^{cut}$, where $p_T^{cut}(\ell)$ and $\not{p}_T^{cut}$ are the charged lepton p_T and the missing transverse momentum threshold. For $M_T \leqslant p_T^{cut}(\ell) + \not{p}_T^{cut}$, the Born cross section vanishes, and the cross section ratio is infinite. The $\mathcal{O}(\alpha^3)$ cross section is small, but non-zero, in this region. The largest contribution to the cross section for $M_T \leqslant p_T^{cut}(\ell) + \not{p}_T^{cut}$ originates from initial state radiation configurations, where the lepton and the neutrino have a small relative opening angle and are balanced by a high p_T photon in the opposite hemisphere. Close to the threshold, $M_T \approx p_T^{cut}(\ell) + \not{p}_T^{cut}$, large logarithmic corrections are present, and for an accurate prediction in this region those corrections need to be resummed. The results of Fig. 8 in this region should therefore be interpreted with caution.

The ratio of the full $\mathcal{O}(\alpha^3)$ and the Born cross section as a function of the transverse mass is shown in Fig. 9. The solid (dashed) lines show the cross section ratio without (with) the lepton identification requirements included. Recombining the electron and photon four-momentum vectors for $\Delta R_{e\gamma} < 0.2$ eliminates the mass singular logarithmic terms and strongly reduces the size of the QED-like final state corrections [see Fig. 9(a)]. These corrections are now of the same size as the initial state QED-like and the modified weak corrections. However, with the total $\mathcal{O}(\alpha)$ EW corrections varying between 1% and 2%, the shape change of the M_T distribution caused by the final state corrections is still significant. For muon final states [see Fig. 9(b)], the cut on the energy of the photon reduces the hard photon part of the $\mathcal{O}(\alpha^3)$ $\mu\nu(\gamma)$ cross section. In this case, the mass singular terms survive and the corrections become larger over the entire range of M_T considered. Before lepton identification requirements are taken into account, the change in the shape of the M_T distribution due to the QED-like final state corrections is more pronounced in the electron channel. Once these requirements are included, the shape change is stronger in the muon case.

The statistical uncertainty in Figs. 8 and 9 due to the Monte Carlo integration procedure is approximately 0.001 for $M_T \leqslant M_W$ and increases to about 0.003 at $M_T = 175$ GeV. Results qualitatively similar to those shown in Figs. 8 and 9 are also obtained for the transverse momentum distribution of the charged lepton.

As we have seen, final state bremsstrahlung has a non-negligible effect on the M_T and $p_T(\ell)$ distribution in the Jacobian peak region. As is well known, electroweak corrections must be included when the W boson mass is extracted from data, otherwise the mass is shifted to a lower value. In the approximate treatment of the electroweak corrections used so far by the Tevatron experiments, only final state QED corrections are taken into account; initial state, interference, and weak correction terms are ignored. Furthermore, the effect of the final state soft and virtual photonic corrections is estimated from the inclusive $\mathcal{O}(\alpha^2)$ $W \to \ell\nu(\gamma)$ width [38] and the hard photon bremsstrahlung contribution [13,14]. When detector effects are included, the approximate calculation leads to a shift of about -50 MeV in the electron case, and approximately -160 MeV in the muon case [15,16].

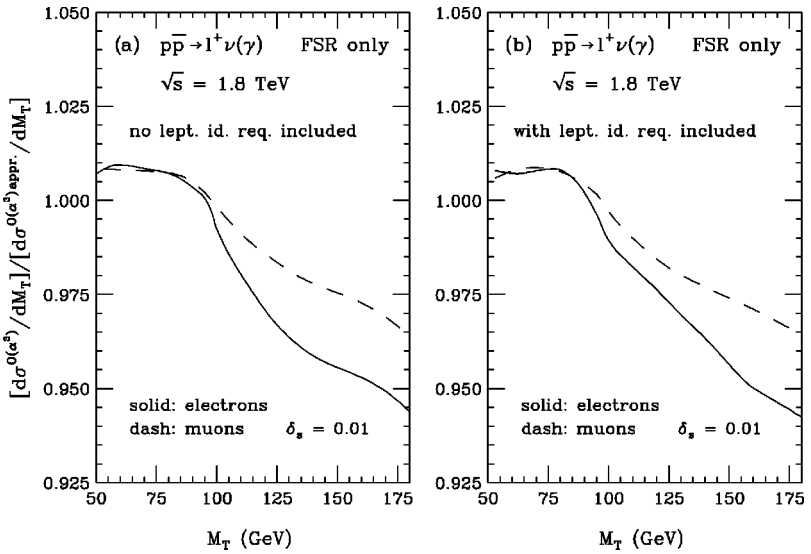

FIG. 10. Ratio of the M_T distributions obtained with the QED-like final state correction part of our calculation to the one obtained using the approximation of Refs. [13] and [14] for $p\bar{p} \to \ell^+\nu(\gamma)$ at $\sqrt{s}=1.8$ TeV (a) without and (b) with lepton identification requirements (see Table I) taken into account. The solid and dashed lines give the results for electron and muon final states, respectively. The approximate NLO transverse mass distribution does depend on δ_s [see Eq. (28)] which is taken to be $\delta_s=0.01$. The cuts imposed are listed in Eqs. (36) and (37). The energy and momentum resolutions used are described in Sec. II C.

Initial state and interference contributions do not change the shape of the M_T distribution significantly (see Fig. 8) and therefore have little effect on the extracted mass. However, correctly incorporating the final state virtual and soft photonic corrections results in a non-negligible modification of the shape of the transverse mass distribution. This is demonstrated in Fig. 10, which shows the ratio of the M_T distribution obtained with the QED-like final state correction part of our calculation to the one obtained using the approximation of Refs. [13] and [14]. The dependence of the ratio on M_T is described by Eq. (28). For $M_T<M_W$, most events originate from the region $\hat{s}\approx M_W^2$, due to the Breit-Wigner resonance. Consequently, there is little dependence of the cross section ratio on M_T in this region. For $M_T>M_W$, the steeply falling cross section in the tail of the Breit-Wigner resonance favors events with $\hat{s}\approx M_T^2$. In this region the term proportional to $\ln(\hat{s}/M_W^2)$ in Eq. (28) causes a change in the shape of the transverse mass distribution. $\Delta\hat{\sigma}^{final}$ also contains a term which is proportional to $\ln(m_\ell^2/M_W^2)$ [see Eq. (28)]. The shape change in the M_T distribution thus is more pronounced in the electron case. Lepton identification requirements have a small effect on the cross section ratio (see Fig. 10). Note that the approximate NLO cross section, and thus the cross section ratio shown in Fig. 10, does depend explicitly on the cutoff δ_s whereas the $\mathcal{O}(\alpha^3)$ cross section resulting from our calculation does not. While the dependence on δ_s is very small for $M_T<M_W$, it is quite pronounced for transverse masses above M_W.

The difference in the line shape of the M_T distribution between the complete $\mathcal{O}(\alpha^3)$ calculation and the approximation used so far occurs in a region which is important for both the determination of the W mass, and the direct measurement of the W width. The precision which can be achieved in a measurement of M_W using the transverse mass distribution strongly depends on how steeply the M_T distribution falls in the region $M_T\approx M_W$ (see Fig. 7). In the region of large transverse masses, $M_T>100-110$ GeV, the shape of the M_T distribution is sensitive to the W width [39]. Any change in the theoretical prediction of the line shape thus directly influences the W mass and width measurements. From a maximum likelihood analysis similar to that carried out in Ref. [21] for Z production, the shift in the measured W mass due to the correct treatment of the final state virtual and soft photonic corrections is found to be $\Delta M_W \approx \mathcal{O}(10\ \text{MeV})$. This shift is much smaller than the present uncertainty for M_W from hadron collider experiments [15,16]. However, for future precision experiments, a difference of $\mathcal{O}(10$ MeV) in the extracted value of M_W can no longer be ignored, and the complete $\mathcal{O}(\alpha^3)$ calculation should be used.

At high luminosities, the transverse mass ratio of W to Z bosons offers advantages in determining the W mass [23,24] over the M_T and $p_T(\ell)$ distributions. The transverse mass ratio of W and Z bosons is defined as

$$R_{M_T}(X_{M_T})=\frac{A_W(X^W_{M_T}=X_{M_T})}{A_Z(X^Z_{M_T}=X_{M_T})}, \tag{39}$$

where A_V $(V=W,Z)$ is the differential cross section

$$A_V(X^V_{M_T})=\frac{d\sigma_V}{dX^V_{M_T}} \tag{40}$$

with respect to the scaled transverse mass,

$$X^V_{M_T}=\frac{M^V_T}{M_V}. \tag{41}$$

The transverse mass of the lepton pair in Z boson events is defined in complete analogy to Eq. (38):

$$M^Z_T=\sqrt{2p_T(\ell^+)p_T(\ell^-)(1-\cos\,\phi)}, \tag{42}$$

where ϕ is the angle between the two charged leptons in the transverse plane.

The ratio of the $\mathcal{O}(\alpha^3)$ and the Born W to Z transverse mass ratio is shown in Fig. 11. To calculate the $\mathcal{O}(\alpha)$ electroweak corrections to Z boson production, we use the results of Ref. [21]. Note that purely weak corrections are not included in this calculation. Identical charged lepton p_T and

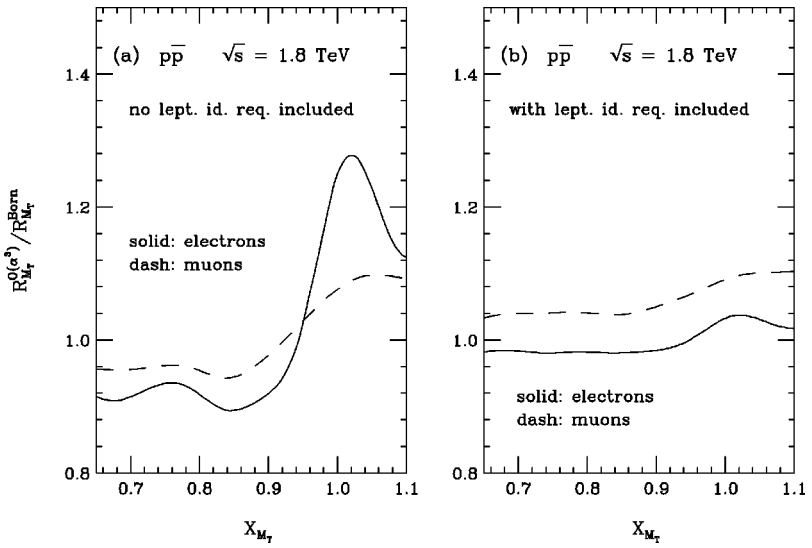

FIG. 11. Ratio of the $\mathcal{O}(\alpha^3)$ and lowest order W^+ to Z transverse mass ratio as a function of the scaled transverse mass, X_{M_T}, at $\sqrt{s}=1.8$ TeV. The solid (dashed) lines show the result for the electron (muon) final state. The ratio without and with lepton identification requirements (see Table I) taken into account is shown in part (a) and part (b) of the figure, respectively. The cuts imposed are listed in Eqs. (36) and (37). The energy and momentum resolutions used are described in Sec. II C. For $p\bar{p}\to\ell^+\ell^-(\gamma)$, we in addition require the di-lepton invariant mass to satisfy the constraint 75 GeV$<m(\ell^+\ell^-)<$105 GeV.

rapidity cuts are used for W and Z production. In the Z boson case, photon exchange and γZ interference effects are included and an additional cut on the di-lepton invariant mass of 75 GeV$<m(\ell^+\ell^-)<$105 GeV has been imposed. In $p\bar{p}\to\ell\nu(\gamma)$ only one of the two leptons can emit a photon, whereas both leptons in $p\bar{p}\to\ell^+\ell^-(\gamma)$ can radiate. The $\mathcal{O}(\alpha)$ corrections are thus significantly larger in the Z case. As a result, the W to Z transverse mass ratio is more strongly affected by electroweak radiative corrections than the M_T^W distribution. Without the lepton identification requirements, the $\mathcal{O}(\alpha)$ corrections increase R_{M_T} by about 30% (10%) at the location of the Jacobian peak ($X_{M_T}=1$) for electrons (muons). For $X_{M_T}<0.9$, the electroweak corrections reduce the transverse mass ratio by 6–10% in the electron case, and by 4–6% in the muon case. The slight dip at $X_{M_T}\approx 0.85$ in Fig. 11(a) is an artifact of the $p_T(\ell)>25$ GeV and $|\eta(\ell)|<1.2$ cuts imposed on the charged leptons in the $Z\to\ell^+\ell^-$ decay [21].

When lepton identification criteria are taken into account, the merging of the electron and photon momentum four vectors for small $e-\gamma$ opening angles again strongly reduces the size of the $\mathcal{O}(\alpha)$ corrections [see Fig. 11(b)]. In the region of the Jacobian peak, the corrections are reduced to $\approx 4\%$, and for $X_{M_T}<0.95$ to about 2% in magnitude. For muon final states, the lepton identification requirements reduce the hard photon part of the $\mathcal{O}(\alpha^3)$ cross sections below the Jacobian peak, but have little effect in the peak region where only few events contain hard photons [see Fig. 9(b)]. The reduction is more pronounced for the $p\bar{p}\to\mu^+\mu^-(\gamma)$ than for the $p\bar{p}\to\mu\nu(\gamma)$ cross section. Consequently, the $\mathcal{O}(\alpha)$ corrections increase R_{M_T} below the Jacobian peak and leave it almost unchanged in the peak region.

B. Electroweak corrections to the W boson cross section and the W to Z cross section ratio

In the past, the measurement of the W and Z boson cross sections has provided a test of perturbative QCD [25,40,41]. With the large data set accumulated in the 1994–95 Tevatron collider run, the uncertainty associated with the integrated luminosity ($\approx 3.6\%$ [41]) became a limiting factor in this measurement. This suggests to use the measured W and Z boson cross sections to determine the integrated luminosity in Run II [41,42]. The cross section ratio

$$R_{W/Z}=\frac{\sigma(p\bar{p}\to W\to\ell\nu X)}{\sigma(p\bar{p}\to Z\to\ell^+\ell^- X)}, \tag{43}$$

together with the theoretical prediction for the ratio of the total W and Z production cross sections, $\sigma_W/\sigma_Z=3.36\pm 0.02$ [43], the LEP measurement of the branching ratio $B(Z\to\ell^+\ell^-)$ and the SM prediction for the $W\to\ell\nu$ decay width, can be used for an indirect determination of Γ_W [25,44]. For integrated luminosities smaller than about 20 fb^{-1}, the W width measurement from $R_{W/Z}$ is expected to yield better results than the direct determination from the M_T distribution [5].

The size of the $\mathcal{O}(\alpha)$ electroweak corrections to the total $p\bar{p}\to\ell\nu X$ cross section and to $R_{W/Z}$ is sensitive to the acceptance cuts and whether lepton identification requirements are taken into account or not. In Table II, we list the electroweak K factor,

TABLE II. The electroweak K-factor $K^{EW}=\sigma^{\mathcal{O}(\alpha^3)}(p\bar{p}\to W\to\ell\nu X)/\sigma^{\rm Born}(p\bar{p}\to W\to\ell\nu)$ ($\ell=e,\mu$) and the correction factor to $R_{W/Z}$, $K_R^{EW}=R^{\mathcal{O}(\alpha^3)}_{W/Z}/R^{\rm Born}_{W/Z}$, with 75 GeV$<m(\ell^+\ell^-)<$105 GeV, for $p\bar{p}$ collisions at $\sqrt{s}=1.8$ TeV. Shown are the predictions without and with the lepton identification requirements of Table I taken into account. The cuts imposed are listed in Eqs. (36) and (37). The energy and momentum resolutions used are described in Sec. II C.

	Without lepton id. requirements	With lepton id. requirements
$K^{EW}(p\bar{p}\to e^+\nu X)$	0.955	0.984
$K^{EW}(p\bar{p}\to\mu^+\nu X)$	0.975	0.947
$K_R^{EW}(e)$	1.032	1.002
$K_R^{EW}(\mu)$	1.012	1.065

$$K^{EW}=\frac{\sigma^{\mathcal{O}(\alpha^3)}(p\bar{p}\to W\to \ell\nu X)}{\sigma^{\rm Born}(p\bar{p}\to W\to \ell\nu)}, \tag{44}$$

and the correction factor for $R_{W/Z}$,

$$K_R^{EW}=\frac{R_{W/Z}^{\mathcal{O}(\alpha^3)}}{R_{W/Z}^{\rm Born}}, \tag{45}$$

for the acceptance cuts listed in Eqs. (36) and (37) with and without taking the lepton identification requirements of Table I into account. As before, we include photon exchange and γZ interference effects, and impose a cut on the dilepton invariant mass of $75\ {\rm GeV}<m(\ell^+\ell^-)<105\ {\rm GeV}$ [21], in the calculation of the $\mathcal{O}(\alpha^3)$ Z boson cross section entering $R_{W/Z}$. It should be noted that the missing purely weak corrections in the calculation of Ref. [21] introduce an uncertainty of $\mathcal{O}(\alpha/\pi)$ in K_R^{EW} which could be significant.

From the results listed in Table II we see that the $\mathcal{O}(\alpha)$ electroweak corrections decrease the W cross section and increase $R_{W/Z}$ by several percent for the cuts imposed. As for the differential cross section, the $\mathcal{O}(\alpha)$ corrections are larger in the electron case when lepton identification requirements are not included. When lepton identification requirements are included, the corrections are reduced in the electron case and enhanced in the muon case. If no acceptance cuts and no lepton identification requirements are taken into account, all mass singular terms cancel in the total cross section, and the size of the electroweak corrections is reduced to about -0.2%.

The size of the $\mathcal{O}(\alpha)$ electroweak corrections should be compared with that of the $\mathcal{O}(\alpha_s)$ and $\mathcal{O}(\alpha_s^2)$ QCD corrections. NLO QCD corrections are known (see e.g. Ref. [45] and references therein) to enhance the W production cross section by about 15–20% and are thus significantly larger than the $\mathcal{O}(\alpha)$ EW corrections. In fact, the size of the $\mathcal{O}(\alpha)$ electroweak corrections to the W cross section when cuts are imposed is about equal to that of the next-to-next-to-leading order (NNLO) QCD corrections [46]. On the other hand, the $\mathcal{O}(\alpha)$ electroweak corrections to $R_{W/Z}$ are in some cases considerably larger than the NLO QCD corrections. Since the QCD corrections to W and Z production are very similar, they cancel almost perfectly in the W to Z cross section ratio; the $\mathcal{O}(\alpha_s)$ corrections to $R_{W/Z}$ are of $\mathcal{O}(1\%)$ or less, depending on the set of parton distribution functions used [46]. In contrast, the electroweak corrections do in general not cancel in $R_{W/Z}$. As noted before, in $Z\to\ell^+\ell^-$ both leptons can emit photons, whereas only the charged lepton radiates in $W\to\ell\nu$ decays. Since final state photonic corrections are the dominating contribution to the $\mathcal{O}(\alpha)$ EW corrections, the $\mathcal{O}(\alpha)$ corrections to the W and Z cross sections are quite different, and thus do not cancel in $R_{W/Z}$. For example, when lepton identification requirements are taken into account, the $\mathcal{O}(\alpha)$ EW corrections in the electron (muon) case increase $R_{W/Z}$ by 0.2% (6.5%). Note that, unlike the electroweak corrections, QCD corrections are only slightly modified by cuts and lepton identification requirements.

From the results shown in Table II we conclude that it will be necessary to correct for higher-order electroweak effects if one wishes to measure the W cross section and $R_{W/Z}$ with an accuracy of $\mathcal{O}(1\%)$ or better.

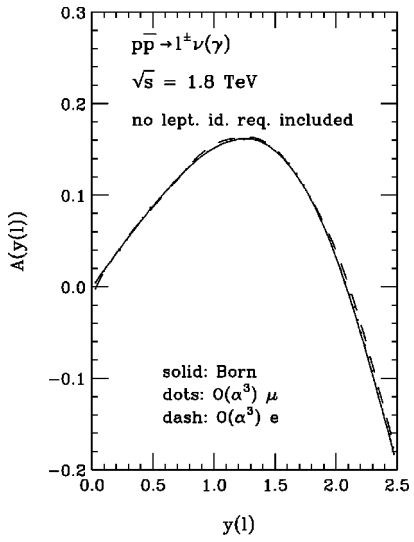

FIG. 12. The charge asymmetry for leptons, $A(y(\ell))$, in $W\to\ell\nu$ decays for $p\bar{p}$ collisions at $\sqrt{s}=1.8$ TeV. The dashed (dotted) lines show the asymmetry for electron (muon) final states including $\mathcal{O}(\alpha)$ electroweak corrections. The solid line gives the Born prediction of $A(y(\ell))$. Except for the pseudorapidity cut on the charged lepton, the cuts listed in Eqs. (36) and (37) are imposed. The lepton identification requirements of Table I are not taken into account. The energy and momentum resolutions used are described in Sec. II C.

C. Electroweak corrections to the charge asymmetry of leptons in W decays

Uncertainties in the parton distribution functions are a major contribution to the systematic error of the W mass extracted in hadron collider experiments [15,16]. Measurement of the charge asymmetry of leptons in W decays [47],

$$A(y(\ell))=\frac{d\sigma^+/dy(\ell)-d\sigma^-/dy(\ell)}{d\sigma^+/dy(\ell)+d\sigma^-/dy(\ell)}, \tag{46}$$

where $y(\ell)$ is the lepton rapidity and

$$\sigma^{\pm}=\sigma(p\bar{p}\to\ell^{\pm}\nu X), \tag{47}$$

provides strong constraints on the ratio of d and u quark distributions [48]. These constraints considerably reduce the uncertainty originating from the parton distribution functions in the W mass measurement [15,16]. It is thus important to know how electroweak radiative corrections affect $A(y(\ell))$. The $\mathcal{O}(\alpha^3)$ asymmetry as a function of the lepton rapidity for $e\nu(\gamma)$ (dashed line) and $\mu\nu(\gamma)$ (dotted line) production is shown in Fig. 12 together with the lowest order prediction (solid line). Except for the pseudorapidity cut on the charged lepton, we impose the cuts listed in Eqs. (36) and (37) in this subsection. Since $A(-y)=-A(y)$, the asymmetry is only displayed for $y(\ell)>0$. The flavor specific lepton identification requirements of Table I are not taken into account in Fig. 12. The asymmetry in the Born approximation for elec-

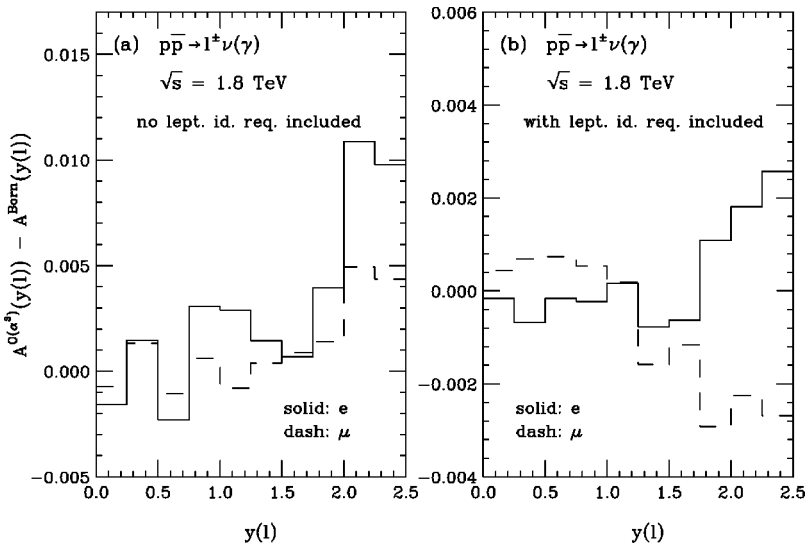

FIG. 13. The difference of the $\mathcal{O}(\alpha^3)$ and the Born charge asymmetry for electrons (solid) and muons (dashed) (a) without and (b) with the lepton identification requirements of Table I taken into account. Except for the pseudorapidity cut on the charged lepton, the cuts listed in Eqs. (36) and (37) are imposed. The energy and momentum resolutions used are described in Sec. II C.

tron and muon final states is virtually indistinguishable for the cuts and the energy and momentum resolutions we use. Electroweak corrections are seen to only slightly affect the charge asymmetry.

In order to display the effect of EW radiative corrections on $A(y(\not{\ell}))$ more clearly, we show the difference between the $\mathcal{O}(\alpha^3)$ and the Born asymmetry in Fig. 13. Without taking the lepton identification requirements of Table I into account, the difference of the $\mathcal{O}(\alpha^3)$ and the Born asymmetry is positive and gradually increases with $y(\not{\ell})$ from zero at $y(\not{\ell})=0$ to about 0.01 for electrons, and approximately 0.005 for muons, at $y(\not{\ell})=2.5$ [see Fig. 13(a)]. Figure 13(b) displays the difference between the $\mathcal{O}(\alpha^3)$ and the Born charge asymmetry when the lepton identification requirements are included in the simulation. Due to the recombination of the electron and photon momentum four vectors for small lepton-photon opening angles, the size of the electroweak corrections to the charge asymmetry in the electron case is drastically reduced when these requirements are taken into account. For $y(e)\leqslant 1.5$, the $\mathcal{O}(\alpha)$ corrections reduce $A(y(e))$ by a very small amount. In the forward rapidity region, $1.7<y(e)<2.5$, the difference of the $\mathcal{O}(\alpha^3)$ and the Born charge asymmetry is positive and slowly increases, reaching approximately 0.0025 at $y(e)=2.5$. For comparison, the statistical error in $A(y(e))$ in this region expected for Run II (assuming $\int \mathcal{L}dt = 2\ \mathrm{fb}^{-1}$) is $\delta A(y=2.5)\approx 0.005$ [36,37]. The variation of the charge asymmetry due to the uncertainties of the present parton distribution functions is about 0.015 [49] in the same region. The magnitude of the $\mathcal{O}(\alpha)$ electroweak corrections for muons and electrons when lepton identification requirements are included is similar. However, in the muon case, the EW corrections enhance (reduce) the $\mathcal{O}(\alpha^3)$ asymmetry at small (large) rapidities.

IV. CONCLUSIONS

The mass of the W boson is one of the fundamental parameters of the SM and a precise measurement of M_W is an important objective for current experiments at LEP2 and future experiments at the Tevatron. A precise measurement of the W mass helps to constrain the Higgs boson mass from radiative corrections. It will also provide restrictions on the parameters of the MSSM. In order to perform such a measurement at a hadron collider, it is crucial to fully control higher order QCD and electroweak corrections. In this paper we have presented a calculation of the electroweak corrections to W production in hadronic collisions which is based on the full set of contributing $\mathcal{O}(\alpha^3)$ Feynman diagrams.

The $\mathcal{O}(\alpha)$ electroweak corrections can be arranged into separately gauge invariant QED-like contributions corresponding to initial state, final state and interference corrections, and gauge invariant modified weak contributions to the W production and decay processes. Due to mass singular logarithmic terms associated with final state photon radiation in the limit where the photon is collinear with one of the leptons, final state radiation effects dominate. Initial state corrections were found to be small after appropriately factorizing the corresponding collinear singularities into the parton distribution functions. However, currently no parton distribution functions which include QED corrections are available. With the factorization scheme used in this paper, the effect of the QED corrections on the PDF is expected to be small. We find that the part of the initial state corrections included in our calculation is uniform over the entire range of the $\not{\ell}\nu$ transverse mass and the lepton p_T range, and increases the differential cross section by about 1%. Likewise, the modified weak corrections are uniform, but decrease the cross section by a similar amount. In contrast, the final state QED-like corrections modify the shape of the M_T and p_T distributions substantially.

Without including the lepton identification requirements imposed by experiments, the effect of the electroweak corrections is larger in the electron channel than in the muon channel. When these requirements are taken into account, the mass singular logarithmic terms are eliminated in the electron case because the electron and photon momentum four vectors are combined for small opening angles where it is difficult to resolve the two particles. Initial state QED-like, final state QED-like, modified weak and interference contributions are then all of similar size. On the other hand, in

order to experimentally identify muons, the energy of the photon is required to be smaller than a critical value if the $\mu-\gamma$ separation is small, and mass singular terms survive. Removing energetic photons thus enhances the effect of the $\mathcal{O}(\alpha)$ corrections, and the effect of the electroweak corrections in the muon case is larger than in the electron case once lepton identification requirements are included.

Electroweak radiative corrections have a significant impact on the W mass extracted from experiment. The main effect is caused by final state photon radiation and is corrected for in the W mass analyses of the Tevatron experiments [15,16]. However, in the calculation used by CDF and DØ [13,14], the effect of the final state soft and virtual photonic corrections is estimated indirectly from the inclusive $\mathcal{O}(\alpha^2)$ $W\to\ell\nu(\gamma)$ width and the hard photon bremsstrahlung contribution. Initial state, interference, and weak contributions to the $\mathcal{O}(\alpha)$ corrections are ignored altogether. The correct treatment of the final state soft and virtual photonic corrections significantly changes the slope of the transverse mass distribution in the region $M_T > M_W$. This changes the W mass extracted from the transverse mass distribution by $\mathcal{O}(10\ \mathrm{MeV})$, and might also have a non-negligible effect on the W width measured from the tail of the M_T distribution. More detailed numerical simulations are needed to quantitatively assess this effect. Initial state, and initial–final state interference corrections, have only a small effect on the M_T distribution and hence are expected to only marginally influence the amount the W boson mass is shifted.

Our results demonstrate that, for the current level of precision, the approximate calculation of Ref. [13] is adequate. The small difference in the W boson mass obtained in the complete $\mathcal{O}(\alpha^3)$ and the approximate calculation, however, cannot be ignored if one attempts to measure the W mass with high precision at hadron colliders. This also raises the question of how strongly multiple final state photon radiation influences the measured W boson mass. So far, only partial calculations exist [50]. A more complete understanding of multiple photon radiation is warranted.

As an alternative to the transverse mass and the lepton p_T distribution, the W to Z transverse mass ratio, R_{M_T}, has been used recently to extract the mass of the W boson. We found that since the $\mathcal{O}(\alpha)$ corrections to the Z boson transverse mass distribution are significantly larger than those to the W M_T distribution, electroweak corrections influence R_{M_T} more strongly than the M_T or $p_T(\ell)$ distribution.

Finally, we studied how electroweak radiative corrections influence the W cross section, the W to Z cross section ratio, $R_{W/Z}$, and the charge asymmetry of leptons in W decays, $A(y(\ell))$. As shown in Table II, the $\mathcal{O}(\alpha)$ electroweak corrections can reduce the W cross section by up to 5% in the presence of cuts. The size of the $\mathcal{O}(\alpha)$ electroweak corrections is of the same order as the NNLO QCD corrections [46]. The $\mathcal{O}(\alpha)$ corrections were found to enhance $R_{W/Z}$ by up to 6.5%. QCD corrections, on the other hand, cancel almost perfectly in the W to Z cross section ratio and are of $\mathcal{O}(1\%)$. The EWK corrections to $R_{W/Z}$ are particularly large in the muon channel when lepton identification requirements are taken into account, due to the cut on the photon energy imposed for small $\gamma-\mu$ opening angles. If photons with higher energies could be tolerated close to the muon without compromising the identification of muons, the size of the $\mathcal{O}(\alpha)$ corrections to $R_{W/Z}$ in the muon channel could be considerably reduced. The $\mathcal{O}(\alpha)$ electroweak corrections to $A(y(\ell))$ may not be negligible in view of the projected accuracy of the charge asymmetry in future Tevatron runs.

ACKNOWLEDGMENTS

We would like to thank I. Adam, M. Demarteau, S. Errede, E. Flattum, H. Frisch, U. Heintz, Y-K. Kim, and E. Laenen for stimulating discussions. U.B. and D.W. are grateful to the Fermilab Theory Group, where part of this work was carried out, for its generous hospitality. This work has been supported in part by Department of Energy Contract No. DE-AC02-76CHO3000 and NSF Grant No. PHY-9600770.

[1] LEP Collaborations, D. Abbaneo *et al.*, Report CERN-PPE/97-154, 1997.

[2] L3 Collaboration, M. Acciarri *et al.*, Phys. Lett. B **431**, 437 (1998).

[3] Particle Data Group, C. Caso *et al.*, Eur. Phys. J. C **3**, 1 (1998).

[4] K. Hagiwara, D. Haidt and S. Matsumoto, Eur. Phys. J. C **2**, 95 (1998); G. Degrassi, P. Gambino, M. Passera, and A. Sirlin, Phys. Lett. B **418**, 209 (1998); G. Degrassi, talk given at the ''*Zeuthen Workshop on Elementary Particle Theory: Loops and Legs in Gauge Theories*,'' Rheinsberg, Germany, 1998, DFPD-98/TH/33.

[5] H. Aihara *et al.*, in ''Future Electroweak Physics at the Fermilab Tevatron: Report of the TEV_2000 Study Group,'' edited by D. Amidei and R. Brock, FERMILAB-Pub-96/082, 1996, p. 63.

[6] U. Baur and M. Demarteau, Proceedings of the Workshop ''*New Directions in High Energy Physics*,'' Snowmass, Colorado, 1996, edited D. G. Cassel, L. Trindle Gennari, and R. H. Siemann, Vol. 1, p. 499.

[7] E. Flattum, FERMILAB-Conf-98/103-E, 1998, to appear in the Proceedings of the ''Recontres de Moriond: QCD and High Energy Hadronic Interactions,'' Les Arcs, France, 1998.

[8] S. Blusk, FERMILAB-Pub/98-151-E, 1998, to appear in the Proceedings of the ''Recontres de Moriond: QCD and High Energy Hadronic Interactions,'' Les Arcs, France, 1998.

[9] P. Chankowski *et al.*, Nucl. Phys. **B417**, 101 (1994); D. Garcia and J. Solá, Int. J. Mod. Phys. A **9**, 211 (1994); W. Hollik, KA-TP-23-1997, 1997, to appear in the Proceedings of the ''International Workshop on Quantum Effects in the MSSM,'' Barcelona, Spain, 1997.

[10] A. Ballestrero *et al.*, in ''Physics at LEP2,'' edited by G. Al-

tarelli, T. Sjostrand and F. Zwirner, CERN Yellow Report CERN-96-01, Vol. 1, p. 141.

[11] J. P. Marriner, Proceedings of the Workshop ''*New Directions in High Energy Physics*'' (Ref. [6]), p. 78; P. P. Bagley *et al.*, *ibid.*, p. 134; D. A. Finley, J. Marriner and N. V. Mokhov, FERMILAB-Conf-96/408, presented at the ''Conference on Charged Particle Accelerators,'' Protvino, Russia, 1996.

[12] S. Keller and J. Womersley, Eur. Phys. J. C **5**, 249 (1998).

[13] F. A. Berends and R. Kleiss, Z. Phys. C **27**, 365 (1985).

[14] R. G. Wagner, Comput. Phys. Commun. **70**, 15 (1992).

[15] CDF Collaboration, F. Abe *et al.*, Phys. Rev. Lett. **75**, 11 (1995); Phys. Rev. D **52**, 4784 (1995); CDF Collaboration, R. G. Wagner, FERMILAB-Conf-97/293-E, to appear in the Proceedings of the ''5th International Conference on Physics Beyond the Standard Model,'' Balholm, Norway, 1997.

[16] DØ Collaboration, S. Abachi *et al.*, Phys. Rev. Lett. **77**, 3309 (1996); DØ Collaboration, B. Abbott *et al.*, Phys. Rev. D **58**, 012002 (1998); *ibid.* **58**, 092003 (1998); Phys. Rev. Lett. **80**, 3008 (1998).

[17] H. Baer, J. Ohnemus, and J. F. Owens, Phys. Rev. D **40**, 2844 (1989); **42**, 61 (1990); L. Bergmann, Ph.D. thesis, Florida State University, 1989; W. Giele and E. W. N. Glover, Phys. Rev. D **46**, 1980 (1992).

[18] D. Wackeroth and W. Hollik, Phys. Rev. D **55**, 6788 (1997).

[19] J. Kripfganz and H. Perlt, Z. Phys. C **41**, 319 (1988); H. Spiesberger, Phys. Rev. D **52**, 4936 (1995).

[20] A. de Rujula, R. Petronzio, and A. Savoy-Navarro, Nucl. Phys. **B154**, 394 (1979).

[21] U. Baur, S. Keller, and W. K. Sakumoto, Phys. Rev. D **57**, 199 (1998).

[22] J. Smith, W. L. van Neerven, and J. A. M. Vermaseren, Phys. Rev. Lett. **50**, 1738 (1983); V. Barger and R. J. N. Phillips, Phys. Lett. **122B**, 83 (1983).

[23] W. T. Giele and S. Keller, Phys. Rev. D **57**, 4433 (1998).

[24] S. Rajagopalan and M. Rijssenbeek, Proceedings of the Workshop ''*New Directions in High Energy Physics*'' (Ref. [6]), p. 537.

[25] DØ Collaboration, S. Abachi *et al.*, Phys. Rev. Lett. **75**, 1456 (1995).

[26] W. Hollik, Fortschr. Phys. **38**, 165 (1990).

[27] T. Kinoshita, J. Math. Phys. **3**, 650 (1962); T. D. Lee and M. Nauenberg, Phys. Rev. **133**, 1549 (1964).

[28] S. Keller and E. Laenen, Report NIKHEF-98-010, 1998.

[29] J. F. Owens and W. K. Tung, Annu. Rev. Nucl. Part. Sci. **42**, 291 (1992).

[30] J. Kubar-Andréé and F. E. Paige, Phys. Rev. D **19**, 221 (1979).

[31] W. A. Bardeen, A. J. Buras, D. W. Duke, and T. Muta, Phys. Rev. D **18**, 3998 (1978).

[32] G. Altarelli, R. K. Ellis, and G. Martinelli, Nucl. Phys. **B157**, 461 (1979); S. Willenbrock, *Proceedings of the Theoretical Advanced Summer Institute (TASI*), Boulder, Colorado, 1989, p. 323.

[33] A. D. Martin, R. G. Roberts, W. J. Stirling, and R. S. Thorne, Eur. Phys. J. C **4**, 463 (1998); A. D. Martin, R. G. Roberts, and W. J. Stirling, Phys. Lett. B **387**, 419 (1996); CTEQ Collaboration, H. Lai *et al.*, Phys. Rev. D **55**, 1280 (1997).

[34] U. Baur and D. Zeppenfeld, Nucl. Phys. **B308**, 127 (1988); Phys. Rev. Lett. **75**, 1002 (1995).

[35] A. D. Martin, R. G. Roberts, and W. J. Stirling, Phys. Rev. D **50**, 6734 (1994).

[36] DØ Collaboration, S. Abachi *et al.*, Report FERMILAB-Pub-96/357-E, 1996.

[37] CDF Collaboration, F. Abe *et al.*, Report FERMILAB-Pub-96/390-E, 1996.

[38] D. Albert, W. J. Marciano, D. Wyler, and Z. Parsa, Nucl. Phys. **B166**, 460 (1980).

[39] CDF Collaboration, F. Abe *et al.*, Phys. Rev. Lett. **74**, 341 (1995).

[40] CDF Collaboration, F. Abe *et al.*, Phys. Rev. D **44**, 29 (1991); Phys. Rev. Lett. **69**, 28 (1992).

[41] CDF Collaboration, F. Abe *et al.*, Phys. Rev. Lett. **76**, 3070 (1996).

[42] M. Dittmar, F. Pauss, and D. Zürcher, Phys. Rev. D **56**, 7284 (1997).

[43] A. D. Martin, R. G. Roberts, and W. J. Stirling, Phys. Lett. B **B228**, 149 (1989).

[44] CDF Collaboration, F. Abe *et al.*, Phys. Rev. Lett. **73**, 220 (1994); Phys. Rev. D **52**, 2624 (1995).

[45] H. Baer and M. H. Reno, Phys. Rev. D **43**, 2892 (1991).

[46] W. L. van Neerven and E. B. Zijlstra, Nucl. Phys. **B382**, 11 (1992).

[47] E. L. Berger, F. Halzen, C. S. Kim, and S. Willenbrock, Phys. Rev. D **40**, 83 (1989).

[48] CDF Collaboration, F. Abe *et al.*, Phys. Rev. Lett. **68**, 1458 (1992); **74**, 850 (1995); R. G. Wagner, FERMILAB-Conf/97-302-E, to appear in the Proceedings of the ''5th International Conference on Physics Beyond the Standard Model,'' Balholm, Norway, 1997.

[49] W. Giele and S. Keller, Phys. Rev. D (to be published), FERMILAB-Pub-98/082-T.

[50] E. Barberio, B. van Eijk, and Z. Was, Comput. Phys. Commun. **66**, 115 (1991); E. Barberio and Z. Was, *ibid.* **79**, 291 (1994).